BubR1 recruitment to the kinetochore via Bub1 enhances Spindle Assembly Checkpoint signaling

Anand Banerjee[1,*, #], Chu Chen[2,*], Lauren Humphrey[2], John J. Tyson[3], Ajit P. Joglekar[2, #]

1 – Academy of Integrated Science, Virginia Polytechnic Institute & State University, Blacksburg, VA 24601, USA

2 – Cell & Developmental Biology, University of Michigan Medical School, Ann Arbor, MI 48109, USA

3 – Department of Biological Sciences, Virginia Polytechnic Institute & State University, Blacksburg, VA 24061, USA

* - These authors contributed equally.

[#] – corresponding authors

Abstract

During mitosis, unattached kinetochores in a dividing cell activate the Spindle Assembly Checkpoint (SAC) and delay anaphase onset by generating the anaphase-inhibitory Mitotic Checkpoint Complex (MCC). These kinetochores generate the MCC by recruiting MCC constituent proteins, including BubR1. In principle, BubR1 recruitment to signaling kinetochores should increase its local concentration and promote MCC formation. However, in human cells BubR1 is mainly thought to sensitize the SAC to silencing; whether BubR1 localization to signaling kinetochores per se enhances SAC signaling activity remains unknown. Therefore, we used ectopic SAC activation systems (eSAC) to isolate two molecules that recruit BubR1 to the kinetochore: the checkpoint protein Bub1 and the KI and MELT motifs in the kinetochore protein KNL1, and observed their contribution to eSAC signaling. Our quantitative analyses and mathematical modeling show that the Bub1-mediated BubR1 recruitment to the human kinetochore promotes SAC signaling and highlight BubR1's dual role of directly strengthening the SAC and indirectly silencing it.

Introduction

The "Spindle Assembly Checkpoint" (SAC) is a cell cycle control that minimizes chromosome missegregation during cell division (Lara-Gonzalez et al., 2021b; Musacchio, 2015). It is activated by kinetochores that are not stably attached to the plus-ends of spindle microtubules. These kinetochores generate a diffusible anaphase-inhibitory signal known as the Mitotic Checkpoint Complex (MCC). The MCC delays anaphase onset to avert cell division in the presence of unattached kinetochores. The rate at which an unattached kinetochore generates MCC depends on its ability to recruit SAC signaling proteins, which include constituent proteins of the MCC: Bub1-Bub3, BubR1-Bub3, Mad1-Mad2, and Cdc20 (Figure 1A, dashed square). This signaling cascade generates either the MCC itself, its sub-complex C-Mad2-Cdc20, or both. Given this knowledge, it is reasonable to expect that the rate of MCC generation at a kinetochore will increase with higher recruitment of signaling proteins, and especially the MCC components, to the kinetochore (Collin et al., 2013; Lara-Gonzalez et al., 2021a; Piano et al., 2021). Interestingly, however, this expectation appears to not hold true for BubR1. Disruption of BubR1 recruitment to unattached kinetochores does not reduce the duration of SAC-induced mitotic arrest in nocodazole-treated cells (Overlack et al., 2015; Zhang et al., 2015). This is because BubR1 recruits to the kinetochore Protein Phosphatase 2A (PP2A), which promotes SAC silencing (Foley et al., 2011; Nijenhuis et al., 2014; Qian et al., 2017). Despite this knowledge, it is crucial to determine whether BubR1 recruitment to the kinetochore promotes SAC signaling by enhancing MCC assembly. This BubR1 activity can be crucial for minimizing chromosome missegregation during normal cell division wherein a small number of unattached kinetochores must activate the SAC and delay anaphase onset (Roy et al., 2020).

In this study, we examine the contribution of BubR1 recruitment to kinetochore-mediated SAC signaling. We first use the ectopic SAC activation system or the 'eSAC' to find that the binding of BubR1 to Bub1 elevates Bub1-mediated MCC generation (Chen et al., 2019). On the other hand, the recruitment of Bub1 and BubR1 via the 'KI' motifs in the kinetochore protein Knl1 does not contribute to MCC generation mediated by the MELT motifs within the Knl1 phosphodomain (Bolanos-Garcia et al., 2011a; Bolanos-Garcia et al., 2011b; Kiyomitsu et al., 2011; Krenn et al., 2012; Primorac et al., 2013; Vleugel et al., 2013; Zhang et al., 2014). We also establish a mathematical model to elucidate the mechanistic details of the SAC signaling cascade that generates the MCC. Finally, we also demonstrate that BubR1 recruitment to the kinetochore via Bub1 promotes SAC signaling.

Results & Discussion

The BubR1 binding domain of Bub1 promotes Bub1-mediated MCC assembly

Bub1 coordinates the rate-limiting step in MCC assembly: the formation of the closed-Mad2-Cdc20 (Mad2:Cdc20) sub-complex (Faesen et al., 2017; Lara-Gonzalez et al., 2021a; Piano et al., 2021). Mad2:Cdc20 must bind BubR1 to complete MCC formation. BubR1 is recruited to the kinetochore by Bub1, and the KI motifs and MELT motifs in KNL1 (Bolanos-Garcia et al., 2011b; Kiyomitsu et al., 2011; Overlack et al., 2015; Zhang et al., 2016). Whether this BubR1 recruitment promotes MCC formation remains unclear. In fission yeast, BubR1 binding to Bub1 is essential for SAC activity (Leontiou et al., 2019). However, BubR1 is unlikely to be recruited to budding yeast kinetochores (Roy et al., 2022; Tromer et al., 2016), and in nocodazole-treated HeLa cells, the disruption of Bub1-mediated BubR1 recruitment slightly strengthens the SAC (Overlack et al., 2015; Zhang et al., 2016) because the disruption of BubR1 recruitment also disrupted BubR1-mediated PP2A recruitment (Elowe et al., 2007; Suijkerbuijk et al., 2012). Therefore, to isolate and quantitatively define the effect of Bub1-BubR1 heterodimerization on Bub1-mediated MCC assembly, we used the ectopic SAC activation system or the eSAC.

Forced dimerization of a fragment of the central domain of Bub1 with Mps1 delays anaphase onset in HeLa cells, budding yeast, and fission yeast (Aravamudhan et al., 2015; Chen et al., 2019; Leontiou et al., 2019; Yuan et al., 2017). In HeLa cells, induced dimerization of the central domain of Bub1 (Bub1$^{231-620}$-mNG-2xFkbp12, diagram in Figure 1B) with the Mps1 kinase domain (Frb-mCherry-Mps1$^{500-817}$) produces a dosage-dependent increase in the duration of mitosis with a maximal duration of ~ 145 minutes (Figure 1C replotted for comparison from (Chen et al., 2019)). Importantly, the extended mitosis was due to increased Mad2-Cdc20 and MCC formation in HeLa cells and fission yeast (Leontiou et al., 2019; Roy et al., 2022). To assess the contribution of Bub1-BubR1 heterodimerization to Bub1-mediated MCC assembly, we created a truncated Bub1 phosphodomain lacking the BubR1 heterodimerization domain (Bub1$^{444-620}$-mNG-2xFkbp12) (Overlack et al., 2015; Zhang et al., 2016). Rapamycin-induced dimerization of this phosphodomain with Frb-mCherry-Mps1^{500-}817 elicited a significantly weaker eSAC activity, with a maximal mitotic duration of 105 ± 6 minutes (Figure 1C, estimated from a fit with the 4-parameter Hill equation, the range indicates 95% confidence intervals, see Methods for details). The absence of the Bub3-binding GLEBS domain in Bub1$^{444-620}$-mNG-2xFkbp12 cannot explain the observed decrease in eSAC activity (Roy et al., 2022). Thus, Bub1-BubR1 heterodimerization promotes MCC mediated by the Bub1 phosphodomain.

98 **Simulation of the signaling activity of the Bub1 phosphodomains**

99 To quantitatively understand how these events shape the dose-response dependence, we
100 constructed a mathematical model by considering the events at the Bub1 eSAC prior to MCC
101 assembly. This model consists of two stages. In the first stage, we calculate the steady-state
102 concentrations of signaling complexes assembled by the Bub1 eSAC phosphodomains assuming
103 mass action kinetics (Figure 1D, equations *1-4, 5a-j*). Bub1$^{231-620}$ recruits BubR1 and Cdc20
104 independently of its phosphorylation state or the presence of other bound proteins; Bub1$^{444-620}$
105 recruits only Cdc20 (Di Fiore et al., 2015; Overlack et al., 2015). Both phosphodomains are
106 activated by Mps1-mediated phosphorylation, after which they recruit Mad1-Mad2 (abbreviated
107 as Mad1/2) (Faesen et al., 2017; Ji et al., 2017). Therefore, the signaling activity of each
108 phosphodomain will be proportional to the amount of Frb-mCherry-Mps1$^{500-817}$, i.e., the eSAC
109 dosage, and it will be limited by the cellular Mad1/2 abundance when the eSAC dosage exceeds
110 Mad1/2 abundance (shown later, see Figure S1A). Using these interactions, Bub1$^{231-620}$ can
111 assemble two types of signaling complexes: one that contains Cdc20, BubR1, and Mad1/2, and
112 one containing only Cdc20 and Mad1/2; Bub1$^{444-620}$ forms only the signaling complex containing
113 Mad1/2 and Cdc20 (Figure 1D, left).

114 We simulated MCC formation by the Bub1:BubR1:Mad1/2:Cdc20 signaling complex as follows.
115 Because Mad2-Cdc20 formation is the rate-limiting step in MCC assembly (Faesen et al., 2017),
116 the Bub1$^{231-620}$:BubR1:Mad1/2:Cdc20 signaling complex first assembles Mad2:Cdc20 with the
117 rate constant k_{asc1}. The newly formed Mad2:Cdc20 can bind BubR1 either within the signaling
118 complex with the rate constant k_{asmcc2} or in the cytosol with the rate constant k_{asmcc1} (Figure 1D,
119 bottom). The model assumes that all the Mad2:Cdc20 formed by Bub1^{231-}
120 ^{620}:BubR1:Mad1/2:Cdc20 binds BubR1 within the signaling complex. However, allowing a
121 reasonable fraction of Mad2:Cdc20 to escape from the signaling complex does not affect the
122 overall behavior of the model. Because Mad2:Cdc20 formation is the rate-limiting step, we reduce
123 the number of free parameters by assuming that k_{asc1} and k_{asmcc2} are equal. The cumulative MCC
124 formed by Bub1$^{231-620}$ is the sum of MCC formed from these two processes. All Mad2-Cdc20
125 generated by Bub1$^{441-620}$:Mad1/2:Cdc20 forms MCC in the cytosol. In the second stage of the
126 model (Figure 1D, equations *5k-n*, Methods), the MCC formed by both processes modulates
127 Cyclin B degradation and thereby controls the timing of metaphase-to-anaphase transition (Figure
128 S1B) (Chen et al., 2019; He et al., 2011).

129 We first simulated the dose-response curve for the Bub1$^{444-620}$ eSAC involving only cytoplasmic
130 MCC assembly. We retained protein concentrations used in the original He et al. model and used

131 reasonable rate constants for Mad2:Cdc20 formation (k_{asc1}) and cytosolic MCC formation (k_{asmcc1},
132 Figure 1E, red curve; see Table S1 for protein concentrations and rate constants used). Next, we
133 considered MCC formation by the Bub1$^{231-620}$ eSAC, which can assemble the MCC within the
134 signaling complex or the cytosol. If BubR1 recruited by the signaling complex does not participate
135 in MCC formation (i.e., k_{asmcc2} = 0), the simulation produced a dose-response curve with a lower
136 maximal response (dotted blue line in Figure 1E). This is because BubR1 bound to Bub1 cannot
137 participate in any form of MCC assembly. Therefore, the only effect of Bub1-BubR1
138 heterodimerization is reduced cytosolic BubR1 concentration, and consequently, reduced rate of
139 MCC generation. This prediction is inconsistent with the data. Therefore, the model predicts that
140 BubR1 recruited by Bub1 must promote MCC formation within the eSAC signaling complex.
141 Following this insight, we assumed that k_{asmcc2} is 10-fold higher than k_{asmcc1} for cytosolic MCC
142 assembly. With this change, the simulation produced a longer delay in anaphase onset, matching
143 our observations.

144 This simulation provides two insights. First, it supports the observation that Bub1-BubR1
145 heterodimerization promotes MCC formation by the eSAC based on the Bub1 phosphodomain. It
146 also indicates that if Bub1-BubR1 heterodimerization does not promote MCC formation, it will lead
147 to BubR1 sequestration and a reduced rate of cytosolic MCC formation. This effect plays a critical
148 role in the experiments that follow.

149

150 **KI motifs suppress the signaling strength of the eSAC phosphodomain**

151 The KI motifs, so named because they contain lysine and iso-leucine residues critical for their
152 activities, recruit Bub1 and BubR1 to the human kinetochore (Figure 1A). The first KI motif (KI1)
153 is thought to exclusively bind Bub1, whereas the second motif (KI2) binds BubR1 (Bolanos-Garcia
154 et al., 2011a; Kiyomitsu et al., 2011; Krenn et al., 2012). A prior study concluded that the KI motifs
155 cooperate with the first MELT motif in KNL1 to strengthen SAC signaling (Krenn et al., 2014;
156 Vleugel et al., 2013). However, it is unclear whether the activity of regulatory enzymes (e.g., PLK1,
157 PP2A) bound to Bub1 and BubR1 plays a role in these observations (Jia et al., 2016; Nijenhuis
158 et al., 2014; von Schubert et al., 2015). Therefore, to test whether Bub1 and BubR1 bound to the
159 KI motifs directly promote MCC assembly and delineate the roles of the KI motifs, we developed
160 an eSAC phosphodomain comprising the two KI motifs and a MELT motif (Knl1$^{160-256}$) (Figure 2A).
161 We also created a variant phosphodomain with inactive KI motifs (Krenn et al., 2012). If Bub1 and
162 BubR1 recruitment via the KI motifs enhances MELT motif activity, this will be apparent as

163 increased signaling strength of this new eSAC phosphodomain compared to the variant
164 phosphodomain with inactive KI motifs.

165 We first determined the dependence of mitotic duration on the dosage of the variant
166 phosphodomain with inactive KI motifs (M1-KI1*-KI2*-mNG-2xFkbp12, Figure 2A left). The
167 maximal response for this phosphodomain was higher than the previously defined maximal
168 response for the eSAC phosphodomain containing the 12th MELT motif alone (211 versus 157
169 minutes with ± 95% confidence intervals of 169-357 and 152-163 respectively predicted by a 4-
170 parameter sigmoidal fit to the binned data). This difference likely results from different Bub1-Bub3
171 binding affinities of the first and twelfth MELT motif (Chen et al., 2019). Interestingly, active KI
172 motifs in the phosphodomain (M1-KI1-KI2) suppressed its signaling strength: the eSAC
173 concentration required for half-maximal response nearly doubled (EC50 = 9.7 and 19.4 a. u.
174 respectively, Figure 2A middle). The decreased apparent signaling strength of the
175 phosphodomain was eventually compensated by high eSAC dosage as evidenced by the maximal
176 mitotic duration at high eSAC dosage (Figure 2A middle and right). These data suggests that the
177 Bub1 and BubR1 molecules recruited by the KI motifs do not enhance eSAC signaling mediated
178 by the upstream MELT motif.

179

180 **Bub1 and BubR1 interactions with the KI motifs do not require Mps1-mediated**
181 **phosphorylation of KNL1**

182 To better understand the observed suppression of eSAC activity by the KI motifs, we constructed
183 a new phosphodomain by fusing an unstructured region of the Knl1 phosphodomain spanning
184 three previously-characterized MELT motifs (Knl1$^{881-1014}$) to the C-terminus of the phosphodomain
185 used above (Knl1$^{160-256}$ also referred to as 'M3', see Figure 2B) (Chen et al., 2019; Vleugel et al.,
186 2015). By incorporating multiple MELT motifs in the phosphodomain, we wanted to test whether
187 the KI motifs influence the ability of the four MELT motifs in the phosphodomain to engage in
188 synergistic signaling (Chen et al., 2019). Based on a previous study, we created mutant
189 phosphodomains wherein the KI motifs were inactive individually or together (KI1*-KI2, KI1-KI2*,
190 and KI1*-KI2*; the asterisk denotes a loss of function, Figure 2B) (Krenn et al., 2012).

191 We first determined whether the two KI motifs interact with Bub1 and BubR1 exclusively and
192 whether the phosphorylation of MELT motifs is necessary for these interactions. We
193 immunoprecipitated the four mNeonGreen-tagged eSAC phosphodomains from whole-cell
194 extracts of mitotic HeLa cells in the absence of the Mps1 kinase domain using mNeonTrap beads

195 and probed the precipitates for Bub1 and BubR1 (Methods). When both the KI motifs were active
196 (KI1-KI2), Bub1 and BubR1 co-precipitated with the eSAC phosphodomain. As expected, Bub1
197 and BubR1 did not co-precipitate with the eSAC phosphodomain containing inactive KI motifs
198 (KI1*-KI2*, Figure 2B). Surprisingly, with the first KI motif inactive (KI1*-KI2), which interacts with
199 Bub1 alone, Bub1 still co-precipitated with the phosphodomain, albeit at a lower level. Moreover,
200 BubR1 coprecipitation was reduced. Inactivation of the second KI motif (KI1-KI2*) made BubR1
201 undetectable in the precipitate and reduced the amount of Bub1. These data are can be explained
202 by the heterodimerization between Bub1 and BubR1, although it remains possible that the second
203 KI motif can interact with Bub1. We obtained similar results from immunoprecipitation experiments
204 involving eSAC phosphodomains with only one MELT motif and the two KI motifs (Supplementary
205 Figure S2A). These experiments show that KI motifs interact with Bub1 and BubR1 constitutively;
206 this interaction does not require the phosphorylation of MELT motifs. They also confirm that the
207 loss-of-function mutants indeed abolish the interactions with Bub1 and BubR1.

208 An N-terminal fragment of KNL1 spanning residues 1-334 transiently localized to kinetochores,
209 likely by interacting with kinetochore-bound Bub1 or BubR1 or with KNL1 itself (Chen et al., 2019;
210 Kern et al., 2015). Therefore, we examined the localization of the KI1-KI2 and the KI1*-KI2*
211 phosphodomain in mitotic cells treated with Rapamycin using immunofluorescence
212 (Supplementary Figure S2B). Both phosphodomains colocalized with kinetochores, although the
213 amount of kinetochore-localized KI1*-KI2* was ~ 20% lower than the KI1-KI2 phosphodomain
214 (Supplementary Figure S2B). Despite this localization, the duration of mitosis for the two cell lines
215 in the absence of Rapamycin was similar to the mitotic duration observed in HeLa cells
216 (Supplementary Figure S2C). We also did not observe defects in chromosome alignment or
217 segregation (Supplementary Figure S2D). Thus, the kinetochore-localized fraction of the
218 phosphodomain does not detectably perturb chromosome biorientation or cell-cycle progression.

219

220 **Bub1 and BubR1 recruited by the KI motifs do not contribute to MCC assembly mediated**
221 **by the MELT motifs**

222 We first determined the baseline activity of the four MELT motifs by establishing the dose-
223 response correlation for the eSAC phosphodomain with inactive KI motifs (KI1*-KI2* in Figure 2B
224 left, purple circles). The response elicited by this eSAC phosphodomain was non-monotonic: the
225 mitotic duration increased steeply before gradually decaying to a lower value (see Supplementary
226 Figure S3A). A non-monotonic response was not apparent for a previously characterized eSAC
227 phosphodomain containing four MELT motifs (numbers 11-14) (Chen et al., 2019). The different

228 behaviors of the two phosphodomains may be ascribed to different Bub1-Bub3 binding affinities
229 of the MELT motifs that they contain. Notably, when both KI motifs were active (KI1-KI2), the
230 maximal duration of mitosis was significantly reduced (~ 87 minutes estimated by 4-parameter
231 sigmoidal fit to the binned averages of the data, see Figure 2C). The KI motifs similarly
232 suppressed the signaling strength of an extended phosphodomain containing 7 MELT motifs
233 (Supplementary Figure S3B).

234 We next determined the response elicited by the two eSAC phosphodomains containing four
235 MELT motifs and only one active KI motif. When only the first KI motif was active (KI1-KI2*, only
236 Bub1 depleted, see Figure 2B), the dose-response data were monotonic with a slightly lower
237 maximal response than the maximal response elicited by KI1*-KI2* (Figure 2C green circles and
238 curve). When only the second KI motif was active (KI1*-KI2, Bub1, and BubR1 depleted, Figure
239 2C), the maximal response was significantly attenuated (blue circles and line in Figure 2C).
240 Interestingly, the response to this eSAC was also non-monotonic, an initial overshoot followed by
241 decay to a lower response level (residuals from the Hill equation fit shown in Supplementary
242 Figure S3A).

243 These results reinforce the conclusion that Bub1 and BubR1 recruited by the two KI motifs do not
244 directly contribute to MCC generation by the MELT motifs within the same phosphodomain
245 (Figure 2C). The distinctly different effects of Bub1 and BubR1 sequestration on eSAC activity
246 also suggest that the cellular abundance of these proteins may be an important aspect of SAC
247 signaling.

248

249 **Numerical simulation of the dose-response data**

250 The strong suppression of eSAC signaling by the second KI motif that binds BubR1 can be
251 ascribed to two effects of BubR1 sequestration: reduced rate of MCC assembly and a lowered
252 limit on the maximal amount of MCC that can be generated. The latter effect is unlikely to play a
253 major role in shaping the observed dose-response data. This is because the KI1*-KI2* eSAC
254 delays mitosis by at most 300 minutes, significantly shorter than ~ 1500 minutes long arrest seen
255 in nocodazole-treated HeLa cells (Collin et al., 2013; Dick and Gerlich, 2013). Therefore, the
256 amount of MCC produced by the eSAC systems is likely to be lower than the amount produced
257 in nocodazole-treated HeLa cells. Therefore, the effect of BubR1 sequestration on the *rate of*
258 *MCC generation rather than the maximal amount of MCC that can be generated* likely shapes the
259 dose-response data.

260 An intuitive explanation for the dose-response dependence can be developed using the following
261 four observations: (1) Bub1 and BubR1 interactions with the KI motifs do not require MELT motif
262 phosphorylation (Figure 2B), (2) Bub1 and BubR1 recruited by the KI motifs do not contribute to
263 the activity of the phosphorylated MELT motifs (Figure 2A-C), (3) the eSAC phosphodomains are
264 significantly more abundant than Bub1 and BubR1 (shown later), and (4) phosphorylated MELT
265 motifs in an eSAC phosphodomain recruit Bub1, BubR1, and Mad1 (Chen et al., 2019). The first
266 three observations indicate that the two KI motifs in the eSAC phosphodomains will differentially
267 sequester Bub1 or BubR1, and the last observation suggests that the MELT motifs in the eSAC
268 phosphodomains will form two distinct signaling complexes: MELpT:Bub1:Mad1/2 and
269 MELpT:Bub1:BubR1:Mad1/2 (Figure 3A; Cdc20 and Mad1/2 are present in both and hence not
270 indicated). When taken together, these observations suggest that the differential sequestration of
271 Bub1 and BubR1 by the KI motifs will affect the composition of the signaling complexes
272 assembled on the phosphodomains. If the two signaling complexes assemble the MCC at
273 different rates, the result will be different mitotic delays explaining why the four phosphodomains
274 produce distinctly different maximal mitotic delays (Dick and Gerlich, 2013). The quantitative
275 dose-response data and numerical simulations provide an excellent opportunity to test this model
276 and the notion that MELpT:Bub1:BubR1:Mad1/2 generates MCC at a higher rate than the
277 MELpT:Bub1:Mad1/2.

278 We simulated this model in two stages (Figure 3A). In the first stage, we calculate the equilibrium
279 concentrations of the two signaling complexes using rates governed by mass action (equations
280 *6-15*, Methods); in the second stage, we calculate the rate of MCC formation and its effect on the
281 metaphase-to-anaphase transition (equations *16-17*, Methods). For both signaling complexes,
282 the events leading up to Mad2:Cdc20 formation are identical. Therefore, we did not explicitly
283 simulate them. After this step, MELpT:Bub1:BubR1 can assemble the MCC either within the
284 signaling complex itself or in the cytosol, whereas MELpT:Bub1 must rely on cytoplasmic MCC
285 assembly. Using these insights, we expanded our previously described eSAC model (Chen et al.,
286 2019). This model simulates the activity of the four MELT motifs in a manner analogous to the
287 original model. Bub1-Bub3 and BubR1-Bub3 complexes are represented by 'Bub1' and 'BubR1'
288 (Figure 3A) (Overlack et al., 2017; Overlack et al., 2015). Activities of the two KI motifs are
289 simulated as protein-protein interactions assuming that KI1 interacts only with Bub1, and KI2
290 interacts with only BubR1 (Figure 3A). Finally, the KI motifs and phosphorylated MELT motifs are
291 assumed to act independently.

292

293 **Dependence of the equilibrium concentrations of MELpT:Bub1 and MELpT:Bub1:BubR1**
294 **assembled by the eSAC systems on Bub1-BubR1 stoichiometry**

295 The equilibrium concentrations of MELpT:Bub1 and MELpT:Bub1:BubR1 depend on two sets of
296 parameters: (1) the concentrations of Bub1, BubR1, and the eSAC phosphodomain (quantification
297 shown after the simulations), (2) the affinities of Bub1 and BubR1 for KI1 and KI2 respectively,
298 Bub1 for phosphorylated MELT motifs, and BubR1 for Bub1 (Krenn et al., 2014; Vleugel et al.,
299 2015; Zhang et al., 2016). We assume that Bub1-BubR1 heterodimerization occurs after Bub1
300 binds MELpT. However, this assumption will not affect the behavior of the model. The values of
301 the parameters used are listed in Table S2.

302 Our first goal was to delineate the effects of the two KI motifs by understanding the reason for the
303 different mitotic durations achieved by KI1*-KI2 and KI1-KI2* at high eSAC dosages. For these
304 phosphodomains to elicit different maximal responses, they must form different amounts of
305 MELpT:Bub1 and MELpT:Bub1:BubR1. Therefore, we investigated how the above two parameter
306 sets affect the equilibrium concentrations of the two signaling complexes formed by KI1*-KI2 and
307 KI1-KI2*. Given a set of affinities of KI1 and KI2 for Bub1 and BubR1, respectively, the
308 concentrations of MELpT:Bub1 and MELpT:Bub1:BubR1 will depend on the relative cellular
309 abundance of Bub1 and BubR1. If BubR1 is much more abundant than Bub1, then nearly every
310 MELpT:Bub1 signaling complex will be able to recruit BubR1 to form MELpT:Bub1:BubR1.
311 Consequently, the concentration of MELpT:Bub1 will become negligible (dashed green and blue
312 lines respectively near the X-axis in Figure 3B, left). At high eSAC dosage, both eSAC systems
313 will form similar amounts of MELpT:Bub1:BubR1 despite the differential sequestration of Bub1
314 and BubR1 (converging dashed lines at high eSAC dosage in Figure 3B, right). Therefore, their
315 eSAC signaling activity will also be similar, contrary to our observations.

316 When BubR1 and Bub1 concentrations are similar, a sizeable fraction of MELpT:Bub1 will not
317 recruit BubR1 (Figure 3B, right, solid lines) especially at a high eSAC dosage. Therefore, at high
318 eSAC dosage, the concentration of MELpT:Bub1:BubR1 is lower for KI1*-KI2 than for KI1-KI2*
319 (solid lines in Figure 3B, left). Figures 3C shows how Bub1-BubR1 stoichiometry affects
320 MELpT:Bub1:BubR1 concentration for the high and constant eSAC dosage (Figure 3C left).
321 BubR1:Bub1 < 2.5 ensures that the two phosphodomains will assembly different concentrations
322 of MELpT:Bub1 and MELpT:Bub1:BubR1 (blue shaded region in Figure 3C left). This difference
323 in the equilibrium concentrations of the signaling complexes can form the basis for differential
324 eSAC activities.

325

326 **A higher rate of MCC generation by MELpT:Bub1:BubR1 compared to MELpT:Bub1 can**
327 **explain the differential behavior of the two phosphodomains**

328 Differences in the concentrations of MELpT:Bub1 and MELpT:Bub1:BubR1 will translate into
329 different activity only if they generate MCC at different rates. As before, we calculate the rate of
330 MCC generation by assuming it to be proportional to the concentrations of MELpT:Bub1 and
331 MELpT:Bub1:BubR1 (Figure 3B). Following our experimental results, the KI-bound Bub1 and
332 BubR1 do not promote eSAC signaling. To simulate the effect of the MCC generated on mitotic
333 progression, we modified the model of metaphase-to-anaphase transition described by He et al.
334 (Figure S4B, Methods) (Chen et al., 2019; He et al., 2011).

335 As discussed in the preceding sections, the maximal mitotic duration produced by the two eSAC
336 systems depends on: (1) the equilibrium concentrations of the MELpT:Bub1 and
337 MELpT:Bub1:BubR1, which are in turn dependent on the Bub1-BubR1 stoichiometry, and (2) the
338 values of the MCC generation rate constants k_{MCC} and k'_{MCC}. To determine the working
339 combination of these factors, we fixed the eSAC dosage at a high value and calculated the
340 duration of mitosis for a range of ratios of k_{MCC} to k'_{MCC} and Bub1:BubR1 stoichiometry. Figure 3D
341 displays how the two ratios affect the maximal duration of mitosis achieved by KI1-KI2* and KI1*-
342 KI2, respectively. In particular, for Bub1:BubR1 ~ 1 and $k_{MCC}/ k'_{MCC} > 6$, the ratio of the maximal
343 mitotic durations achieved by the KI1-KI2* and KI1*-KI2 eSAC systems exceed 1.4.

344 Following this result, we used [Bub1]:[BubR1] = 1 and $k_{MCC}:k'_{MCC} = 0.1$ (rate constant for MCC
345 assembly within the signaling complex is 10-fold higher than the rate constant for cytoplasmic
346 MCC assembly) to simulate the dose-response curves for all four phosphodomains. This
347 simulation captures key characteristics of the dose-response data for all four phosphodomains
348 (Figure 3E). As before, the assumption of synergistic signaling was necessary to reproduce the
349 non-monotonicity of the dose-response data for the phosphodomain containing four MELT motifs
350 (Chen et al., 2019). Without it, the responses elicited by all phosphodomains become monotonic
351 (Figure S4D).

352

353 **Stoichiometry of Bub1, BubR1, Mad1, and the eSAC phosphodomain in HeLa cells**

354 The relative amounts of Bub1, BubR1, and the eSAC phosphodomain emerge as critical
355 determinants of eSAC signaling. Therefore, for comparative protein abundance measurements,
356 we constructed genome-edited HeLa cell lines wherein mNeonGreen (abbreviated as mNG) was
357 fused to the N-terminus of Bub1 and BubR1 and the C-terminus of Mad1. In all three cases, we

358 obtained heterozygous cell lines with partially edited genomes. Consequently, approximately half
359 of the protein in these cells was labeled (Figure 4A, Methods).

360 Quantitation of mNG fluorescence in mitotic cells revealed that the KI1-KI2 phosphodomain was
361 2-4-fold more abundant than the three SAC proteins (Figure 4B, Methods). Therefore, and given
362 the constitutive activity of the two KI motifs, the eSAC phosphodomains containing active KI motifs
363 will deplete Bub1 and BubR1 from the cytosol. The measurements also show that BubR1 is ~ 2-
364 fold more abundant than Bub1 and Mad1 (Figure 4B). In the case of BubR1, the measured
365 abundance includes free BubR1-Bub3 and BubR1-Bub3 incorporated into MCC. Although the
366 fraction of free BubR1-Bub3 remains unknown, this value is likely to be less than 2-fold higher
367 than that of Bub1-Bub3, consistent with the requirement of comparable amounts of Bub1-Bub3
368 and BubR1-Bub3 in our simulations.

369

370 **Recruitment of BubR1 by Bub1 per se strengthens kinetochore-based SAC signaling**

371 Following these results and insights, we re-examined the role of Bub1-BubR1 heterodimerization
372 in kinetochore-based SAC signaling. PP2A recruitment to the kinetochore in this manner
373 contributes to SAC silencing directly (Espert et al., 2014; Kruse et al., 2013; Qian et al., 2017),
374 and indirectly by either promoting PP1 recruitment (Nijenhuis et al., 2014) or stabilizing
375 kinetochore-microtubule attachment (Suijkerbuijk et al., 2012). Therefore, we created two BubR1
376 mutants: mNG-BubR1$^{\Delta KARD}$ that lacks the PP2A-binding KARD domain and mNG-BubR1$^{\Delta HD, \Delta KARD}$
377 that additionally lacks the BubR1 heterodimerization domain (Figure 5A). The complete removal
378 of KARD in these mutants is expected to abolish the binding of B56α and other isoforms of B56
379 onto BUBR1 (Wang et al., 2016a; Wang et al., 2016b) enabling us to analyze whether the
380 recruitment of BUBR1 to the signaling kinetochore *per se* contributes to the SAC activity.
381 Importantly, we ensured that the expression level of these mutants was similar to wildtype BubR1
382 because the transient over-expression of BubR1 can deplete the cytosolic pool of Bub3 (Taylor
383 et al., 1998) and adversely affect the SAC or even induce cell death (data not shown). Higher
384 cytosolic BubR1 concentration may also proportionally increase the rate of cytosolic MCC
385 formation and thus mask impaired MCC assembly within the kinetochore.

386 We knocked down endogenous BubR1 in HeLa-A12 using RNA interference and rescued these
387 cells with mNG-BubR1$^{\Delta KARD}$ or mNG-BubR1$^{\Delta HD, \Delta KARD}$. As expected, mNG-BubR1 $^{\Delta KARD}$ localized
388 to unattached kinetochores, whereas mNG-BubR1$^{\Delta HD, \Delta KARD}$ localization to unaligned kinetochores
389 was undetectable (Figure 5A). We also quantified the duration of mitotic arrest using nocodazole

390 treatment following the previous studies. To ensure that the BubR1 mutants were not over-
391 expressed, we established the physiological BubR1expression level by quantifying cytosolic
392 BubR1 fluorescence in the genome-edited *mNG-BUBR1* HeLa-A12 cells treated with control
393 siRNA and imaged under identical conditions. In our knock-in/knock-down experiments, we
394 considered only those cells exhibiting mNG intensity that is 0.5–2-times the average mNG
395 intensity of mitotic mNG-BubR1 HeLa-A12 cells (Figure 5B, left). Quantification of mitotic duration
396 revealed that cells expressing mNG-BubR1$^{\Delta KARD}$ arrested significantly longer than control cells;
397 the longer duration is attributable to the loss of PP2A activity from the kinetochores (Saurin et al.,
398 2011). Notably, cells rescued with mNG-BubR1$^{\Delta HD,\ \Delta KARD}$ arrested for a significantly shorter
399 amount of time compared to the cells rescued with mNG-BubR1$^{\Delta KARD}$ (Figure 5B, right). Thus, the
400 recruitment of BubR1 *per se* strengthens the SAC.

401 In conclusion, Bub1-BubR1 heterodimerization significantly enhances SAC signaling activity in
402 human cells. This enhancement may be simply due to enrichment of BubR1 at the site of
403 formation of Mad2-Cdc20 (Lara-Gonzalez et al., 2021a; Piano et al., 2021), although more
404 complicated mechanisms can also be envisioned. Bub1 and BubR1 recruitment via the KI motifs
405 does not contribute to eSAC signaling mediated by MELT motifs indicating that their contribution
406 to SAC signaling is likely to be minor. Although prior studies found that the KI motifs promote SAC
407 signaling, this contribution was detectable only in the context of recombinant Knl1 variants
408 containing either just one MELT motif (Krenn et al., 2014) or three inactive MELT motifs (Vleugel
409 et al., 2013); the contribution was undetectable in a Knl1 variant containing multiple MELT motifs
410 but lacking the N-terminus including the KI motifs (Zhang et al., 2014). Compared to the KI motifs,
411 phosphorylated MELT motifs bind significantly more strongly to Bub1 and BubR1 (Krenn et al.,
412 2012; Primorac et al., 2013; Zhang et al., 2016). MELT motifs also vastly outnumber the KI motifs.
413 Therefore, phosphorylated MELT motifs recruit the majority of Bub1 and BubR1 to the kinetochore
414 (Vleugel et al., 2015; Zhang et al., 2014). Our findings highlight the dual effect of Bub1-mediated
415 BubR1 recruitment on the SAC. BubR1 stabilizes the kinetochore-microtubule attachment by
416 recruiting PP2A, thereby promotes the silencing of SAC. But it also promotes the SAC activity per
417 se, which is critical for minimizing chromosome missegregation in normally dividing cells, wherein
418 the last few unattached kinetochores need to be able to signal the cell to delay anaphase onset
419 (Roy et al., 2020).

420
421
422

Acknowledgements

This work was supported by R35-GM126983 from NIGMS to APJ. We thank Dr. Stephen S. Taylor for the generous gift of antibodies, Dr. Eugene Makeyev for the HeLa acceptor cell line, and Dr. Michael Lampson for plasmids. We also thank members of the Joglekar lab for stimulating discussions. The use of the Incucyte system was made possible by a generous gift from the Richard Tam Foundation to Prof. Sue O'Shea (Cell & Developmental Biology, University of Michigan Medical School).

MATLAB codes used for the simulations and for generating figure panels can be accessed on GitHub: https://github.com/anandban/eSAC-KI)

The authors declare that no competing financial interests exist.

435 **Materials and Methods**

436 **Plasmid construction**

437 The plasmids used for the stable cell lines were based on plasmids that have been described
438 previously (Chen et al., 2019). Briefly, the phosphodomain was integrated into either *Not*I or *Asc*I
439 and *Xho*I restriction sites to create constitutively expressed phosphodomain-mNeonGreen-
440 2xFkbp12. The Mps1$^{500-857}$ fragment corresponding to the Mps1 kinase domain was integrated
441 into the *Fse*I and *Bgl*II restriction sites to create conditionally expressed Frb-mCherry-Mps1$^{500-857}$.
442 eSAC phosphodomains spanning the 1st MELT motif (M1) and the two KI motifs were created by
443 fusing Knl1$^{160-256}$ to mNeonGreen-2xFkbp12. eSAC phosphodomains containing four MELT
444 motifs and the two KI motifs were created by fusing Knl1$^{160-256}$ to Knl1 fragment Knl1$^{881-1014}$
445 spanning MELT motifs 12-14, which has been characterized previously (Vleugel et al., 2015). The
446 activity of the first KI motif was disrupted by changing its amino acid sequence from
447 'K**I**D**TT**S**F**LANLK' to 'KADAASALANLK' (KI1*). Similarly, the activity of the second KI motif was
448 disrupted by mutating its amino acid sequence from 'KIDFND**F**IK**R**LK' to 'KIDFNDAIKALK' (KI2*)
449 following (Krenn et al., 2012).

450 DNA repair templates used for CRISPR/Cas9 mediated genome editing were constructed via
451 DNA assembly using the NEB HiFi DNA assembly kit per the manufacturer's instructions.
452 Successfully edited alleles encode mNeonGreen-tagged SAC proteins that separate the
453 corresponding wildtype protein and the fluorescent protein mNeonGreen by a short flexible linker
454 (mNG-BUBR1 and mNG-BUB1: GSGGSG; MAD1-mNG: GGAGGSGG). The sequences of all
455 homology-directed repair template plasmids and Cre-lox recombination-mediated cassette
456 exchange plasmids are available upon request.

457

458 **Tissue culture and cell line construction for eSAC analyses**

459 Henrietta Lacks (HeLa) cells were grown in DMEM media supplemented with 10% FBS, 1%
460 Pen/Strep, 1x-Glutamax, and 25 mM HEPES under standard tissue culture conditions (37 °C and
461 5% CO2). Stable cell lines expressing the two eSAC components were generated by integrating
462 a bi-cistronic eSAC plasmid at engineered *lox* sites in the HeLa genome according to the protocol
463 described in (Khandelia et al., 2011). Upon transfection, DMEM media supplemented with 1 µg/ml
464 Puromycin was used to select transformed cells, and all the colonies were pooled to culture the
465 transformed cells used in the experiments.

466 To conduct dose-response analysis, each eSAC cell line was plated ~ 40-48 hours prior to the
467 start of the experiment in DMEM media without Puromycin. Doxycycline was added at the time of
468 plating to induce the expression of Frb-mCherry-Mps1. Prior to imaging, the cells were washed

469 with PBS. Fluorobrite media with 10% FBS 1% Pen/Strep with or without Rapamycin were added
470 to each well.
471
472 **Genome editing HeLa cells using CRISPR/Cas9**
473 The guide RNAs (gRNAs) for in situ BUBR1 and BUB1 N-terminal mNeonGreen-tagging were 5'-
474 CAGGAUGGCGGCGGUGAAGA-3' and 5'-GGUUCAGGUUUGGCCGCUGC-3', respectively.
475 The gRNA for in situ MAD1 C-terminal mNeonGreen-tagging was 5'-
476 CAGACCGUGGCGUAGCCUGC-3'. Single guide RNAs (sgRNAs) were synthesized using the
477 EnGen sgRNA Synthesis Kit (for the *Streptococcus pyogenes*-originated Cas9, New England
478 Biolabs). The SpCas9-sgRNA ribonucleoprotein (RNP) complex was assembled at room
479 temperature in a buffer consisting of 20 mM of HEPES-KOH (pH 7.5), 150 mM of KCl, 1 mM of
480 $MgCl_2$, ten percent (by volume) of glycerol, and 1 mM of DTT using 100 pmol of SpCas9- 2×NLS
481 (the QB3 MacroLab) and 120 pmol of sgRNA. The RNP complex and 1.5 µg of a linearized
482 homology-directed repair template plasmid were transfected into 2×10^5 – 5×10^5 nocodazole-
483 arrested mitotic HeLa A12 cells using a Nucleofector and the associated Cell Line Kit R (Lonza)
484 following manufacturer's instructions. After five weeks, green fluorescence-positive mitotic cells
485 (arrested by 330 nM of nocodazole for 16 hours) were sorted directly into 96-well plates at 1
486 cell/well. Healthy colonies were subject to further validation by genotyping and sequencing, as
487 well as immunoblotting.
488 For genotyping, HeLa-A12 genomic DNAs were purified using the Wizard SV Genomic DNA
489 Purification System (Promega). Genotyping primers (BUBR1 forward primer 5'-
490 CCTGGTCACATCTGAGCTAT-3', BUBR1 reverse primer 5'-CTCAGTGAGACTCCAGTGTT-3',
491 BUB1 forward primer 5'-CCCTCTACATGAAGGCGCTA-3', BUB1 reverse primer 5'-
492 GCTCGCCCAAGGTAAACATT-3', MAD1 forward primer 5'-GGACTTTTCAGGGACGTGGT-3',
493 and MAD1 reverse primer 5'-GAGTTGGGAGGAGGGGACTC-3') were designed to bind outside
494 of homology arms to avoid false-positive colonies from integration of the homology-directed repair
495 template plasmid to an off-target genomic locus.
496
497 **Drug and RNAi treatments**
498 To induce the expression of the mCherry-Frb-Mps1 kinase domain doxycycline was added to a
499 final concentration of 2 ug/ml (stock concentration 2 mg/ml in DMSO) ~ 48 hours prior to the start
500 of the experiment. Prior to prior to the start of each experiment, Rapamycin was added ~ 1 hour
501 of the experiment to a final concentration of 500 nM (stock concentration 500 µM in DMSO) to
502 induce the dimerization of the eSAC kinase domain with the eSAC phosphodomain. Nocodazole

503 was added to the final concentration of 330 nM (stock concentration 330 μM in DMSO). The
504 cocktail of siRNA against five different B56 isoforms was added to a final concentration of 40 nM
505 (stock concentration 10 μM). The siRNA sequences were obtained from ref. (Nijenhuis et al.,
506 2014). Cell cycle synchronization was in G1/S was achieved by treating cells with 2.5 mM
507 thymidine (from a 100 mM stock in PBS) for 16-18 hours. Cells were washed with DMEM for
508 release from the G1/S arrest. To arrest cells in a prometaphase-like condition, cells were released
509 from a G1/S block and then treated with 236 nM GSK923295 (stock concentration 236 μM in
510 DMSO) ~ seven hours post-release and imaged after one hour.
511
512 **Immunoprecipitation**
513 HeLa A12 cells constitutively expressing either MELT1-KI or MELT1-KI-M3 were synchronized at
514 G1/S by 2.5 mM of thymidine. 9 hours after being released from the (double) thymidine block,
515 cells were synchronized in metaphase using 10 μM MG132. After another 1.5 hours, cells were
516 scraped off the plate, washed once with PBS, pelleted, snap-frozen, and stored at −80 °C. Cells
517 were thawed, resuspended in the complete lysis buffer (75 mM HEPES-HCl (pH 7.5), 150 mM
518 KCl, 1.5 mM EGTA, 1.5 mM MgCl2, 10% (by volume) glycerol, and 0.075% (by volume) Nonidet
519 P-40 (AmericanBio); immediately before use one cOmplete protease inhibitor cocktail tablet
520 (EDTA-free, Roche Diagnostics) and a phosphatase inhibitor cocktail (1 mM $Na_4P_2O_7$, 0.1 mM
521 Na_3VO_4, 5 mM NaF, and 2 mM sodium β-glycerophosphate) were added), and lysed for 1 hour at
522 4 °C while rotating. Cell lysates were then centrifuged at 18,000 g for 25 min at 4 °C. The
523 supernatant was subsequently cleared by control agarose beads for 1.5 hours at 4 °C to reduce
524 non-specific binding. Cleared supernatant was then mixed with mNeonGreen-Trap agarose
525 beads (ChromoTek) and rotated for 1.5 hours at 4 °C. Beads were washed 4 times using the lysis
526 buffer. Finally, 2×Laemmli buffer (Bio-Rad Laboratories) supplemented with β-mercaptoethanol
527 was added to the beads. Samples were boiled in a water bath for 10 min before subjecting to
528 SDS-PAGE. The following antibodies and working dilutions were used in immunoblotting:
529 SB1.3 antibody against BUB1 (Taylor et al., 2001), 1:500 or 1:1000, sheep polyclonal; BUB3
530 antibody (Sigma B7811), 1:500, rabbit polyclonal; FKBP12 antibody (Abcam ab2918), 1:2000,
531 rabbit polyclonal; BUBR1 antibody (Bethyl A300-995A), 1:1000, rabbit polyclonal.
532
533 **Immunofluorescence**
534 HeLa cell lines were grown on sterile coverslips in 6 well plates in media supplemented
535 with 1 μg/ml Doxycycline to induce the expression of mCherry-Frb-Mps1 kinase domain.

536 After ~ 48 hours, the cells were treated with 500 nM Rapamycin. After four hours of
537 incubation, cells were fixed with 4% paraformaldehyde and stained with ACA antibodies
538 (1:1000, Antibodies Inc., Davis, CA) and Alexa-633-conjugated secondaries (1:5000).
539 After staining, the cells were embedded in Diamond mounting media and stored at room
540 temperature.
541 The mounted cells were imaged on an Eclipse Ti-E/B inverted microscope (Nikon) with a CFI
542 Plan Apochromat VC 100 ×, 1.40 NA oil objective (Nikon). The microscope was equipped with a
543 H117E1 motorized stage (Prior Scientific), a NanoScanZ 100 piezo stage (Prior Scientific), and
544 an X-Light V2 L-FOV confocal unit with 60 μm pinholes (CrestOptics). A CELESTA Light Engine
545 (Lumencor) served as the excitation laser source, featuring a 477-nm line for imaging the
546 mNeonGreen protein, 546-nm line for imaging mCherry, and 647-nm line for imaging the Alexa-
547 633-conjugated antibodies. Fluorescence emission light was filtered by ET605/52m (Chroma
548 Technology) for the red channel and by ET525/36m (Chroma Technology) for the green channel.
549 Images were acquired by a Prime 95B 25mm sCMOS camera (Teledyne Photometrics). A custom
550 MATLAB program was used to quantify kinetochore-localized fluorescence signals.
551

552 **Long term live-cell imaging of HeLa cells**

553 Imaging was conducted as described in detail previously (Chen et al., 2019). We used either the
554 Incucyte Zoom live cell imaging system (Sartorus) or the ImageXpress Nano live cell imaging
555 system (Molecular Devices), both equipped with a 20x Phase objective. To image cells on the
556 Incucyte system, cells were plated in 12-well plastic tissue culture plates, whereas they were
557 plated in 24-well plate glass-bottom dishes (Corning) for the ImageExpress Nano system. At each
558 position, one phase, GFP, and mCherry image was acquired every 10 minutes. The exposure
559 times for mCherry and GFP images were adjusted to minimize photobleaching while enabling
560 accurate determination of intensity values. It should be noted that the excitation sources, optics,
561 and detector on the ImageXpress Nano and the Incucyte microscope are entirely different.
562 Therefore, the mCherry intensity values across different experiments are not directly comparable.
563

564 **Image analysis**

565 Prior to intensity quantification, acquired images were pre-processed using functions from the
566 'Image Processing Toolbox' provided with Matlab as follows. First, the phase image sequence
567 was registered to remove any movement of the field of view between adjacent timepoints, and at
568 each timepoint, the same transform was applied to the GFP and mCherry images to register them.

569 Additionally, image intensity from a blank, unseeded well was used for background correction of
570 the fluorescence channels. Next, GFP and mCherry fluorescence signals were quantified using a
571 custom graphical user interface (GUI) written in Matlab as described previously. Briefly, this
572 interface uses cross-correlation of each phase image with a circular kernel to identify cells with
573 circular shapes close to the diameter of the circular kernel. The centroids of these shapes were
574 then linked along the time axis. These images were presented to the user via the GUI to (a)
575 discard false positive, non-mitotic cells or debris and (b) visually correct the time of entry into or
576 exit from mitosis. The GUI then calculated the GFP and mCherry signals per cell as the average
577 fluorescence intensity.
578 In all the dose-response assays discussed in this study, the phosphodomain is highly and
579 constitutively, expressed in all cells, whereas the kinase domain is expressed conditionally by an
580 inducible promoter. Consequently, the amount of the kinase domain expressed varies from cell
581 to cell, and it is lower than the amount of the phosphodomain in most cells. Because of this design
582 of the eSAC system, the dosage of the dimerized signaling complex in a cell can be inferred from
583 the amount of Frb-mCherry-Mps1$^{500\text{-}817}$ in that cell. Therefore, we defined the dosage of the eSAC
584 signaling complex by quantifying the average mCherry fluorescence within a cell and the
585 response as the duration of mitosis (the amount of time that the cell spends with a spherical
586 morphology that is characteristic of mitotic HeLa cells).

587 The Hill equation is used to fit the sigmoidal trend:

588 $$Time\ in\ mitosis\ =\ m\ +\ \frac{M}{1+(\frac{EC50}{[eSAC\ activator]})^{n}},$$

589 wherein *n* is the Hill coefficient and *EC50* is the level of the eSAC activator at which the time in
590 mitosis reaches the middle between the baseline level (*m*) and the plateau level (*m* + *M*).
591

592 **Statistical analysis**

593 To determine the overall trend in the dose-response data, the data were first binned (in MATLAB),
594 and then the mean values of each bin were overlayed on the data. The number of observations
595 and technical replicates are noted in the figure legends. These mean values were fit with a four-
596 parameter sigmoidal curve using the GraphPad Prism 9 software. Statistical significance of the
597 difference between the mean values in Figure 5B was assessed using the unpaired t-test with
598 Welch's correction.
599
600

601 **Mathematical modeling**

602 **Modeling the activity of Bub1 phosphodomains**

603 **Stage 1: Calculation of the steady-state concentrations of signaling complexes**

604 (MATLAB codes available on GitHub: https://github.com/anandban/eSAC-KI)

605 This model simulates the eSAC activity of the Bub1$^{221\text{-}620}$ and Bub1$^{441\text{-}620}$ phosphodomains. In the
606 equations below, we refer to these phosphodomains simply as 'Bub1'. The eSAC activator
607 complex is formed by the dimerization of Bub1 with the Mps1 kinase domain ($\mathrm{Bub1{:}Mps1}$). Once
608 Mps1 phosphorylates Bub1, Bub1 can bind Mad1/2 ($\mathrm{Bub1{:}Mps1{:}Mad1/2}$). Therefore, the
609 concentrations of different species of Bub1 are related by the equation:

610 $$[\mathrm{Bub1}]_{\mathrm{T}} = [\mathrm{Bub1{:}Mps1{:}Mad1/2}] + [\mathrm{Bub1{:}Mps1}] + [\mathrm{Bub1}]. \quad (1)$$

611 Assuming reversible binding between phosphorylated Bub1 and Mad1/2 complex, the
612 concentration of eSAC activator complex will saturate to a value dependent on the finite
613 concentration of Mad1/2 (set at 100 nM, Fig. S1A). Note that Bub1 can produce MCC only if it
614 recruits Mad1/2. Therefore, even though Bub1:Mps1 and Bub1 can both bind BubR1 and Cdc20,
615 they do not participate in SAC signaling. The recruitment of SAC proteins, formation of signaling
616 complexes, and MCC are calculated by assuming mass action kinetics.

617 Model of Bub1-mediated MCC formation:

618 Available data suggest that a signaling complex comprising Bub1$^{221\text{-}620}$, BubR1, Mad1, and Cdc20
619 facilitates the formation of either Mad2:Cdc20 or the MCC. We assume that when BubR1 is
620 present the phosphodomain assembles MCC, and when BubR1 is absent, the phosphodomain
621 produces Mad2:Cdc20. Therefore, the rate of Mad2:Cdc20 and MCC formation is calculated as:

622 $$\text{Mad2:Cdc20 formation rate at the Bub1}^{231\text{-}620}\text{ phosphodomain}$$
623 $$= k_{\mathrm{asmcc2}} \cdot [\mathrm{Mad2}]_{\mathrm{I}} \cdot [\mathrm{Cdc20{:}Bub1{:}Mad1/2}] \quad (2)$$

624 $$\text{MCC formation rate at the Bub1}^{231\text{-}620}\text{ phosphodomain}$$
625 $$= k_{\mathrm{asmcc2}} \cdot [\mathrm{Mad2}]_{\mathrm{I}} \cdot [\mathrm{Cdc20{:}Bub1{:}Mad1/2{:}BubR1}], \quad (3)$$

626 where,

627 $[\mathrm{Mad2}]_{\mathrm{I}}$ = the concentration of inactive (open) form of Mad2 in the cytoplasm

628 $[\mathrm{Cdc20{:}Bub1{:}Mad1/2}]$ = the concentration of the complex between Bub1, Mad1, and Cdc20.

629 $[\mathrm{Cdc20{:}Bub1{:}Mad1/2{:}BubR1}]$ = the concentration of the complex between Bub1, BubR1,
630 Mad1, and Cdc20.

For the sake of simplicity, we assume that the rate constant for MCC formation (k_{asmcc2}) is numerically equal to the rate constant for Mad2:Cdc20 formation. This assumption is consistent with the observation that Mad2:Cdc20 formation is the rate-limiting step in MCC formation (Faesen et al., 2017).

The cytosolic Mad2:Cdc20 molecules produced by either phosphodomain interact with cytosolic, free BubR1 to complete MCC formation. We denote the rate constant for this reaction byk_{asmcc1}. Therefore, the rate of cytosolic MCC formation is calculated as:

$$\text{MCC formation rate in the cytoplsam} = k_{\mathrm{asmcc1}} \cdot [\mathrm{BubR1}]_{\mathrm{f}} \cdot [\mathrm{Mad2{:}Cdc20}], \quad (4)$$

where,

$[\mathrm{BubR1}]_{\mathrm{f}}$ = the concentration of free BubR1 in the cytoplasm.

Stage 2: Effect of MCC formation on the timing of metaphase-to-anaphase transition

We used a previously described model of metaphase-to-anaphase transition to simulate the effect of the MCC generated on the duration of mitosis (Chen et al., 2019; He et al., 2011). In this model (schematic at the top of Figure S1B), Cyclin B ('CycB') is synthesized at a constant rate and degraded upon APC:Cdc20-dependent ubiquitination (denoted simply as Cdc20). The abundance of CycB determines the activity of CDK1:CycB complexes, which in turn determines the activity of the eSAC complexes via phosphorylation. CDK1:CycB activity is antagonized by the counter-acting protein phosphatase PP2A:B56 ('CAPP') (Bouchoux and Uhlmann, 2011; Sullivan et al., 2004). This scheme is consistent with recent data revealing that CDK1:CycB phosphorylates Bub1 to promote its interaction with Mad1 (Ji et al., 2017). Furthermore, Mps1 kinase activity is also downregulated by PP2A (Espert et al., 2014; Hayward et al., 2019). This scheme regulates the amount of active eSAC.

The active eSAC ultimately produces MCC according to the scheme discussed in detail above with BubR1 as an MCC component. Therefore, we modified the original model to include BubR1 as well as the dissociation of MCC into its constituent proteins (shown by the red dashed arrow in Figure S1B). Furthermore, active APC:Cdc20 promotes the inactivation of closed/active Mad2 in MCC; this positive feedback of active Cdc20 on its own release from the MCC accelerates the activation of APC:Cdc20 during the transition into anaphase (Chen et al., 2019; He et al., 2011).

The equations for this model are given below using the following notation:

$$\mathrm{eS1} \sim \mathrm{Bub1{:}\,Mps1{:}\,Mad1/2}$$

$$\text{eS2} \sim \text{Bub1: Mps1: Mad1/2: Bub1: BubR1}$$

$$\frac{d[\text{eS1}_\text{I}\text{: Cdc20}]}{dt} = k_{\text{fcdc}}[\text{eS1}_\text{I}] \cdot [\text{Cdc20}] - k_{\text{rcdc}}[\text{eS1}_\text{I}\text{: Cdc20}] + k_{\text{dies2}}[\text{eS2}_\text{I}\text{: Cdc20}] + k_{\text{dies2}}[\text{eS2}_\text{A}\text{: Cdc20}] \quad 5(a)$$

$$\frac{d[\text{eS1}_\text{A}]}{dt} = k_{\text{ancyc}}[\text{eS1}_\text{I}] \cdot [\text{CycB}] - k_{\text{incapp}}[\text{eS1}_\text{A}] \cdot [\text{CAPP}] - k_{\text{ases2}}[\text{eS1}_\text{A}] \cdot [\text{BubR1}] + k_{\text{dies2}}[\text{eS2}_\text{A}] - k_{\text{fcdc}}[\text{eS1}_\text{I}] \cdot [\text{Cdc20}] + k_{\text{rcdc}}[\text{eS1}_\text{A}\text{: Cdc20}] + k_{\text{asmcc2}}[\text{eS2}_\text{A}\text{: Cdc20}] \cdot \text{Mad2I} + k_{\text{asc1}}[\text{eS1}_\text{A}\text{: Cdc20}] \cdot \text{Mad2I} \quad 5(\text{b})$$

$$\frac{d[\text{eS1}_\text{A}\text{: Cdc20}]}{dt} = k_{\text{fcdc}}[\text{eS1}_\text{A}] \cdot [\text{Cdc20}] - k_{\text{rcdc}}[\text{eS1}_\text{A}\text{: Cdc20}] - k_{\text{asc1}}[\text{eS1}_\text{A}\text{: Cdc20}] \cdot \text{Mad2I} \quad 5(\text{c})$$

$$\frac{d[\text{eS2}_\text{I}]}{dt} = -k_{\text{ancyc}}[\text{eS2}_\text{I}] \cdot [\text{CycB}] + k_{\text{incapp}}[\text{eS2}_\text{A}] \cdot [\text{CAPP}] - k_{\text{fcdc}}[\text{eS2}_\text{A}] \cdot [\text{Cdc20}] + k_{\text{rcdc}}[\text{eS2}_\text{I}\text{: Cdc20}] \quad 5(d)$$

$$\frac{d[\text{eS2}_\text{I}\text{: Cdc20}]}{dt} = -k_{\text{dies2}}\,[\text{eS2}_\text{I}\text{: Cdc20}] + k_{\text{fcdc}}[\text{eS2}_\text{I}] \cdot [\text{Cdc20}] - k_{\text{rcdc}}[\text{eS2}_\text{I}\text{: Cdc20}] \quad 5(e)$$

$$\frac{d[\text{eS2}_\text{A}]}{dt} = k_{\text{ases2}}\,[\text{eS1}_\text{A}] \cdot [\text{BubR1}] - k_{\text{dies2}}\,[\text{eS2}_\text{A}] + k_{\text{ancyc}}\,[\text{eS2}_\text{I}] \cdot [\text{CycB}] - k_{\text{incapp}}\,[\text{eS2}_\text{A}] \cdot [\text{CAPP}] - k_{\text{fcdc}}\,[\text{eS2}_\text{I}] \cdot [\text{Cdc20}] + k_{\text{rcdc}}[\text{eS2}_\text{A}\text{: Cdc20}] + k_{\text{asc1p}}[\text{eS2}_\text{A}] \cdot \text{Mad2I} \quad 5(\text{f})$$

$$\frac{d[\text{eS2}_\text{A}\text{: Cdc20}]}{dt} = -k_{\text{dies2}}\,[\text{eS2}_\text{A}\text{: Cdc20}] + k_{\text{fcdc}}[\text{eS2}_\text{A}] \cdot [\text{Cdc20}] - k_{\text{rcdc}}[\text{eS2}_\text{A}\text{: Cdc20}] - k_{\text{asc1}}[\text{eS1}_\text{A}\text{: Cdc20}] \cdot \text{Mad2I} - k_{\text{asmcc2}}[\text{eS2}_\text{A}\text{: Cdc20}] \cdot \text{Mad2I} - k_{\text{asc1p}}[\text{eS2}_\text{A}] \cdot \text{Mad2I} \quad 5(\text{g})$$

$$\frac{d[\text{Bub1X:BubR1}]}{dt} = k_{\text{ases2}}[\text{Bub1X}] \cdot [\text{BubR1}] - k_{\text{dies2}}[\text{Bub1X:BubR1}] - k_{\text{fcdc}}[\text{Bub1X:BubR1}] \cdot [\text{Cdc20}] + k_{\text{rcdc}}[\text{Bub1X: Cdc20: BubR1}] \quad 5(h)$$

$$\frac{d[\text{Bub1X: Cdc20}]}{dt} = k_{\text{fcdc}}[\text{Bub1X}] \cdot [\text{Cdc20}] - k_{\text{rcdc}}[\text{Bub1X: Cdc20}] - k_{\text{ases2}}[\text{Bub1X: Cdc20}] \cdot [\text{BubR1}] + k_{\text{dies2}}[\text{Bub1X:Cdc20:BubR1}] \quad 5(i)$$

$$\frac{d[\text{Bub1X: Cdc20: BubR1}]}{dt} = k_{\text{fcdc}}\,[\text{Bub1X: BubR1}] \cdot [\text{Cdc20}] + k_{\text{ases2}}\,[\text{Bub1X: Cdc20}] \cdot [\text{BubR1}] - k_{\text{dies2}}\,[\text{Bub1X:Cdc20:BubR1}] - k_{\text{rcdc}}[\text{Bub1X: Cdc20: BubR1}] \quad 5(j)$$

$$\frac{d[\text{CycB}]}{dt} = k_{\text{scyc}}\,\text{CycBM} - k_{\text{dcyc}} \cdot [\text{CycB}] + k_{\text{dcyc20}} \cdot [\text{Cdc20}] \cdot [\text{CycB}] \quad 5(k)$$

$$\frac{d[\text{Mad2A:Cdc20}]}{dt} = k_{\text{asc1}}[\text{Mad2I}] \cdot [\text{eS1}_\text{A}\text{: Cdc20}] - k_{\text{dic1}}[\text{Mad2A: Cdc20}] - k_{\text{asmcc1}}[\text{Mad2A:Cdc20}] \cdot [\text{BubR1}] \quad 5(l)$$

$$\frac{d[\text{MCC}]}{dt} = k_{\text{asmcc2}}[\text{Mad2I}] \cdot [\text{eS2}_\text{A}\text{: Cdc20}] + k_{\text{asmcc1}}[\text{Mad2A: Cdc20}] \cdot [\text{BubR1}] - (k_{\text{dimcc}} + k_{\text{imad20}} \cdot [\text{Cdc20}]) \cdot [\text{MCC}] \quad 5(m)$$

$$\frac{d[\text{CAPP}]}{dt} = k_{\text{acapp}}([\text{CAPP}]_\text{T} - [\text{CAPP}]) - k_{\text{icapp}}[\text{CycB}] \cdot [\text{CAPP}] \quad 5(\text{n})$$

688 The molecular species, chemical reactions, parameters, and constraints involved in the model
689 are presented in an Excel file and Table S1 (Supporting Information). A MATLAB script was used
690 to read this file and produce a file with Ordinary Differential Equations (ODEs) describing the rate
691 of change of all molecular species. We numerically integrated the ODEs to calculate the time
692 evolution of [CycB] and the other molecular species. For the initial conditions of species involving
693 BubR1 and Cdc20 bound to Bub1 phosphodomain (both signaling and non-signaling) we used
694 the equilibrium concentrations. These concentrations depend on the concentration of eSAC
695 activator complex and were calculated at the start of each simulation. The initial concentrations
696 of the following species were kept constant: [CycB] = 45 nM, [Mad2:Cdc20] = 0 nM, [MCC] = 25
697 nM, [CAPP] = 5 nM. In the simulation, the system evolves towards a steady state corresponding
698 to anaphase (low [CycB] and high [Cdc20]). We assume that a cell exits mitosis when [CycB]
699 drops below 1 nM (Fig. S1E). If the initial conditions are metaphase-like (high [CycB] and low
700 [Cdc20]), small variations in the initial conditions does not qualitatively affect the outcome of the
701 model. Furthermore, the main result of this analysis – Bub1-BubR1 produces MCC at a higher
702 rate than Bub1 – is robust, even though many different combinations of parameters produce
703 similar looking dose:response curves.
704
705 **Modeling the activities of eSAC phosphodomains containing four MELT motifs and the KI**
706 **motifs**
707 This model simulates the dose-response data for the eSAC systems involving MELT and KI
708 motifs. As before, the simulation takes place in two stages. In the first stage, we calculate the
709 steady-state concentrations of SAC signaling proteins (Bub1 and BubR1) bound to the
710 phosphorylated MELT motifs and KI motifs of an eSAC phosphodomain. This is followed by
711 calculation of MCC generation using the steady-state concentrations of MELpT:Bub1 and
712 MELpT:Bub1:BubR1. In the second stage, we simulate the duration of mitosis, according to the
713 overall reaction scheme developed by He et al.
714
715 **Stage 1: Simulation of SAC protein recruitment by the eSAC phosphodomains**
716 <u>Rules for protein-protein interactions:</u>
717 The phosphodomain consists of four MELT motifs and either active or inactive KI motifs. All four
718 MELT motifs in phosphodomains complexed with the Mps1 kinase domain are assumed to be
719 phosphorylated. They can recruit Bub1, which represents Bub1-Bub3 in this model. Upon binding
720 to the MELT motif, Bub1 recruits BubR1 representing BubR1-Bub3. The KI1 motif can bind to
721 Bub1, whereas the KI2 motif can bind BubR1. We assume that MELT and KI motifs in the eSAC

722 phosphodomain interact with SAC proteins independently. The KI-bound Bub1 and BubR1 do not
723 participate in SAC signaling. Therefore, the KI motifs act as sinks that reduce free Bub1 and
724 BubR1 concentrations. We assigned the same rate of binding of the 'Bub1' protein to each MELT
725 motif (*kf* in Table S2), but assigned a low unbinding rate (*kr*, Table S2) for the strong MELT motifs
726 (MELT 1, 12 and 14), and a higher unbinding rate for the weak MELT motif (MELT 13) following
727 previous studies (Chen et al., 2019; Vleugel et al., 2015). We also chose the dissociation constant
728 for KI1:Bub1 binding to be equal to the dissociation constant for the KI2:BubR1 binding.
729
730 <u>Calculation of the steady-state concentrations of signaling complexes:</u>
731 This model avoids unnecessary complexity by assuming that the rate of MCC formation is simply
732 proportional to the number of phosphorylated MELT motifs that recruit Bub1 or both Bub1 and
733 BubR1. This simplification is justified, because the recruitment of Mad1, Mad2, and Cdc20 is
734 independent of BubR1 recruitment. Thus, the main goal is to determine the steady-state
735 concentrations of the two distinct signaling complexes: MELpT:Bub1 or MELpT:Bub1:BubR1.
736 This calculation is performed as follows.
737 Each phosphorylated MELT motif can be in one of three possible states: MELpT (unbound MELT),
738 MELpT:Bub1 (MELT bound by Bub1), and MELpT:Bub1:BubR1 (MELT bound by Bub1 and
739 BubR1). Since there are four MELT motifs in each eSAC activator complex, the number of
740 possible states for the phosphomimic become 3^4 = 81. The time evolution of concentrations of
741 different Bub1 and BubR1 bound states of eSAC activator complex is given by:

742 $$\dot{\mathbf{X}} = \mathbf{AX} \tag{6}$$

743 where $\mathbf{X} = \{x_1, x_1, \dots, x_N\}$ is a vector of concentrations of the $N = 81$ different Bub1 and BubR1
744 binding states of the phosphodomain, and **A** is the rate matrix.
745 Similarly, each KI motif of the phosphodomain can be in two states: bound or unbound. The
746 binding of Bub1 and BubR1 to KI motifs is described by the set of equations:
747

748 $$\dot{y}_1 = k_{\mathrm{fbub}} \cdot [\mathrm{Bub1}]_{\mathrm{f}} \cdot (\mathrm{KI_T} - y_1) - k_{\mathrm{rbub}} \cdot y_1 \tag{7}$$

749 $$\dot{y}_2 = k_{\mathrm{fbubr}} \cdot [\mathrm{BubR1}]_{\mathrm{f}} \cdot (\mathrm{KI_T} - y_2) - k_{\mathrm{rbubr}} \cdot y_2 \tag{8}$$

750 where, $\mathrm{KI_T}$ is the total concentration of KI motifs, and

751 $$y_1 = [\mathrm{KI1{:}Bub1}],$$

752 $$y_2 = [\mathrm{KI2{:}BubR1}].$$

753 $[\mathrm{Bub1}]_\mathrm{f}$ and $[\mathrm{BubR1}]_\mathrm{f}$ are the cytoplasmic concentrations of free Bub1 and BubR1, respectively.
754 The parameters k_fbub and k_rbub are the binding and unbinding rate constants between Bub1 and
755 the first KI1, and the parameters k_fbubr and k_rbubr are the binding and unbinding rates between
756 BubR1 and KI2.

757 The concentrations satisfy the constraints:

758 $$[\mathrm{eSAC}] = \sum_{i=1}^{N} x_i \tag{9}$$

759 $$[\mathrm{Bub1}]_\mathrm{T} = [\mathrm{Bub1}]_\mathrm{f} + y_1 + \sum_{i=1}^{N} n_i \cdot x_i \tag{10}$$

760 $$[\mathrm{BubR1}]_\mathrm{T} = [\mathrm{BubR1}]_\mathrm{f} + y_2 + \sum_{i=1}^{N} m_i \cdot x_i \tag{11}$$

761 Here, x_i is the concentration of the i-th species, n_i = number of Bub1 bound to i-th species of the
762 phosphodomain, and m_i = number of BubR1 units bound to the i-th species. We assume
763 $[\mathrm{Bub1}]_\mathrm{T} = 100\ \mathrm{nM}$ and $[\mathrm{BubR1}]_\mathrm{T} = 100\ \mathrm{nM}$. The equilibrium concentration of each state was
764 obtained by numerically solving

765 $$\dot{\mathbf{X}} = 0, \mathrm{i} = 1,2,\ldots,81 \text{ and } \dot{y}_j = 0, j = 1,2$$

766 In experiments, the concentration of eSAC activator complex is measured in arbitrary units of
767 mCherry fluorescence (a. u.), whereas in our model the unit of concentration is nano moles (nM).
768 In our simulations, we chose the maximum value of concentration of eSAC activator complex (the
769 value corresponding to 20 a. u. in experiments) to be 200 nM. For easier comparison to
770 experimental figures, in our simulation results the eSAC activator complex concentration is
771 expressed in arbitrary units, with 1 a. u. of fluorescence corresponding to 10 nM.
772 Figure S4A shows the abundance of different Bub1 and BubR1-bound states as functions of the
773 total concentration of eSAC activator complex for KI1*-KI2*. At low eSAC concentrations, the
774 eSAC tends to be highly loaded, with Bub1 and BubR1 on every MELT motif. However, for cells
775 with a high eSAC concentration, [eSAC] >> $[\mathrm{Bub1}]_\mathrm{T}$, the most abundant eSAC species is one that
776 does not bind any Bub1 at all (not shown), followed by species that bind either Bub1 or Bub1-
777 BubR1 at only one of the four MELT motifs. We define the sum of concentration of MELpT:Bub1
778 and MELpT:Bub1:BubR1 as $[\mathrm{eSAC}]_\mathrm{T}$:
779

780 $$[\mathrm{eSAC}]_\mathrm{T} = [\mathrm{MELpT{:}Bub1}] + [\mathrm{MELpT{:}Bub1{:}BubR1}] \tag{12}$$

$$[\text{MELpT:Bub1}] = \sum_{i=1}^{N} (n_i - m_i) \cdot x_i \tag{13}$$

$$[\text{MELpT:Bub1:BubR1}] = \sum_{i=1}^{N} m_i \cdot x_i \tag{14}$$

Formation of MCC by the eSAC signaling complexes

We assume that the MELpT:Bub1 and MELpT:Bub1:BubR1 complexes catalyze the assembly of MCC at the apparent rates constants k_{MCC} and k'_{MCC}. A schematic diagram of the molecular mechanism underlying this model is displayed in Figure 4A.

We assume that the recruitment of SAC proteins (Bub1 and BubR1) to MELT motifs of the eSAC activator complexes enables the incorporation of Cd20 into MCC. Since different species catalyze this reaction at different rates, we define the effective rate of conversion, k_{asmcc}, as the concentration-weighted sum of the conversion rates of each eSAC complex:

$$k_{\text{asmcc}} = \frac{1}{[\text{eSAC}]_{\text{T}}} \cdot \left[k_{\text{MCC}} \cdot \sum_{i=1}^{N} (n_i - m_i) \cdot x_i \; + \; k'_{\text{MCC}} \cdot \sum_{i=1}^{N} m_i \cdot x_i \right], \tag{15}$$

where k_{MCC} and k'_{MCC} are the MCC formation rates due to MELpT:Bub1 and MELpT:Bub1:BubR1, respectively. Note, for most species, the rate of MCC generation is additive. For example, $k_{0012} = k_{\text{MCC}} + k'_{\text{MCC}}$ for a phosphodomain that binds only Bub1 at the 13th MELT motif and Bub1:BubR1 at 14th MELT motif (Table S3). Using $[\text{eSAC}]_{\text{T}}$ and k_{asmcc} as inputs for the He model (discussed below), we calculated the time evolution of Cyclin B concentration and from it the time in mitosis.

Stage 2: The effect of MCC produced on exit from mitosis

To calculate the effect of MCC generated by the eSAC on mitotic exit, we used a simplified version of the model of the mitotic checkpoint proposed by the He model (He et al., 2011). Active eSAC signaling complexes (eSAC_{A}) generate MCC, as described in the previous section. The temporal dynamics of our mitotic checkpoint model are determined by the ordinary differential equations.

$$\frac{\text{d}[\text{CycB}]}{\text{d}t} = k_{\text{scyc}} - \left(k_{\text{dcyc}} + k_{\text{dcyc,c20}} \cdot [\text{Cdc20}]\right) \cdot [\text{CycB}] \tag{16a}$$

$$\frac{\text{d}[\text{eSAC}_{\text{A}}]}{\text{d}t} = k_{\text{ancyc}} \cdot [\text{CycB}] \cdot ([\text{eSAC}]_{\text{T}} - [\text{eSAC}_{\text{A}}]) - k_{\text{in,capp}} \cdot [\text{CAPP}] \cdot [\text{eSAC}_{\text{A}}] \tag{16b}$$

$$\frac{\mathrm{d}[\mathrm{MCC}]}{\mathrm{d}t} = k_{\mathrm{asmcc}} \cdot [\mathrm{Cdc20}] \cdot [\mathrm{eSAC}]_{\mathrm{A}} - \left(k_{\mathrm{dimcc}} + k_{\mathrm{imad}} + k_{\mathrm{imad,c20}} \cdot [\mathrm{Cdc20}]\right) \cdot [\mathrm{MCC}] \qquad (16c)$$

$$\frac{\mathrm{d}[\mathrm{CAPP}]}{\mathrm{d}t} = k_{\mathrm{acapp}} \cdot ([\mathrm{CAPP}]_{\mathrm{T}} - [\mathrm{CAPP}]) - k_{\mathrm{icapp,cyc}} \cdot [\mathrm{CycB}] \cdot [\mathrm{CAPP}] \qquad (16d)$$

In these equations, $[\mathrm{CycB}] = [\mathrm{CDK{:}CycB}]$, $[\mathrm{Cdc20}] = [\mathrm{APC{:}Cdc20}]$, $[\mathrm{eSAC}]_{\mathrm{T}}$ is the total concentration of Bub1 and BubR1-bound eSAC signaling complexes (Eq. 10), which is either in the active, signaling-competent state $\mathrm{eSAC_A}$, or the inactive state, $[\mathrm{eSAC_I}] = [\mathrm{eSAC}]_{\mathrm{T}} - [\mathrm{eSAC_A}]$. [MCC] and [CAPP] refer to the concentrations of the mitotic checkpoint complex and the CDK-counteracting protein phosphatase, respectively. In addition, the total concentration of Cdc20 is:

$$[\mathrm{Cdc20}]_{\mathrm{T}} = [\mathrm{Cdc20}] + [\mathrm{MCC}] \qquad (17)$$

The values of the parameters in the model and of the fixed concentrations of some components, as listed in Table S2, are taken from (He et al., 2011).

<u>Simulation of time in mitosis</u>

To determine the timing of the metaphase-to-anaphase transition, we assume that a cell exits mitosis when [CycB] drops below 1 nM. We numerically integrated Ordinary Differential Equations (ODEs) to calculate the time evolution of [CycB] and the components of the cell cycle machinery. As before, the initial conditions for the simulation are chosen to be [CycB] = 45 nM, $[\mathrm{eSAC_A}] = 0$, [MCC] = 25 nM, and [CAPP] = 5 nM. The qualitative aspects of our results do not depend on the initial conditions. Figure S3C displays typical time courses for [CycB], for different eSACs, for [eSAC activator complex] = 10 a. u. The system always comes out of mitosis (as seen by the drop in [CycB]), albeit after different time delays.

833 **Figure 1**

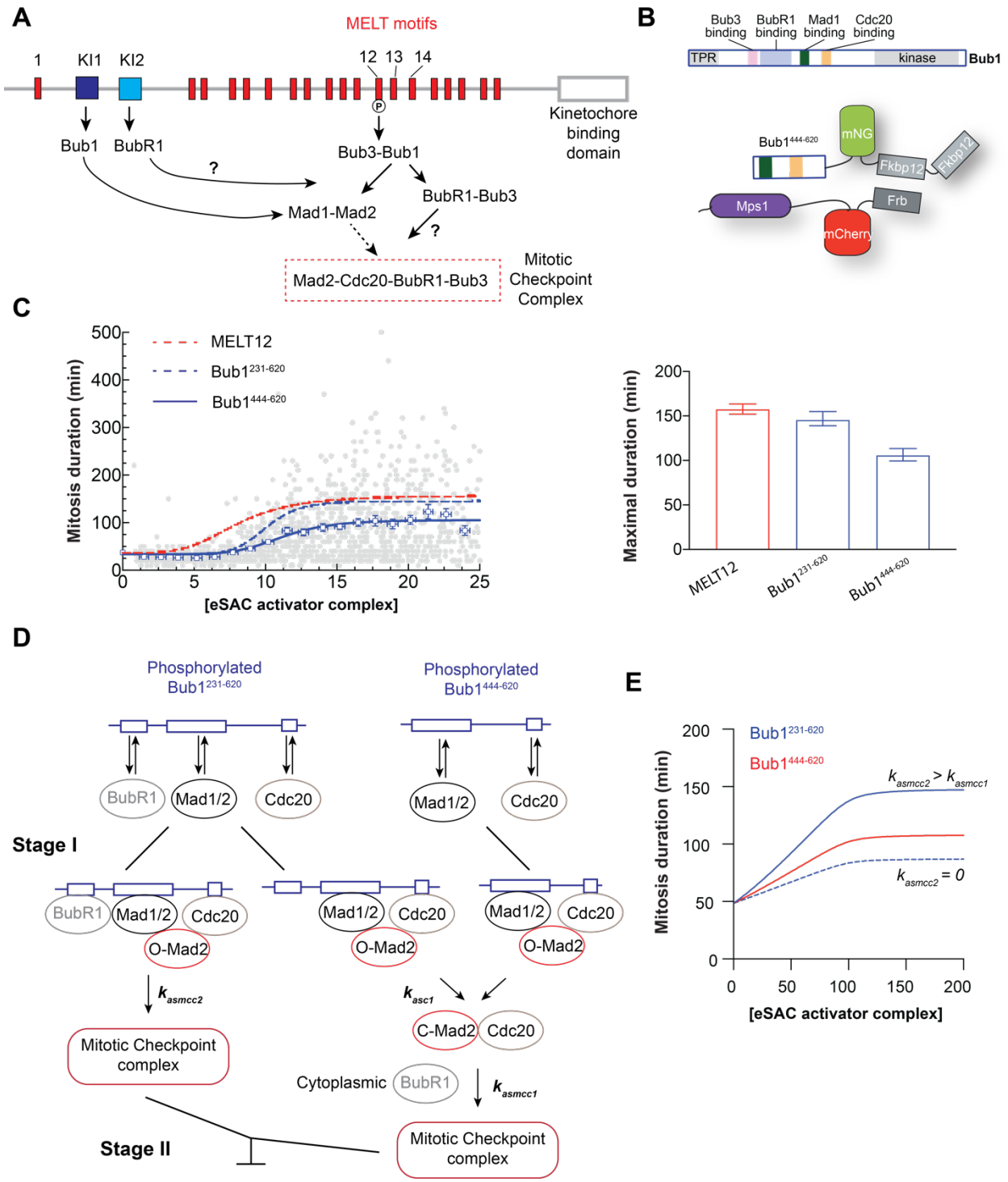

834

835 **Figure 1 The contribution of Bub1-BubR1 heterodimerization to MCC assembly in eSAC**

836 **signaling.**

837 **A** Schematic at the top displays the domain organization of human Knl1. Below is a simplified
838 schematic displaying the pathways that recruit SAC signaling proteins to unattached
839 kinetochores.
840 **B** Schematic at the top displays the domain organization of human Bub1. The cartoon
841 represents the ectopic SAC activation (eSAC) system.
842 **C** Dose-response data for an eSAC system that uses $Bub1^{444-620}$ as the phosphodomains.
843 Each gray circle represents a single cell (n = 1920 from 2 experiments; 139 and 155 are
844 the lower and upper 95% confidence intervals). The blue squares represent the mean
845 values of the dose-response data binned according to mCherry fluorescence. Vertical and
846 horizontal lines represent SEM. The solid blue curve displays the least squares 4-
847 parameter sigmoidal fit to the binned mean values. Hill equation fits for dose-response
848 data for one MELT motif (MELT12, dashed red curve) and an extended $Bub1^{231-620}$
849 phosphodomain containing the Bub3- and BubR1-binding sites (dashed blue curve) from
850 our previous study have been super-imposed for comparison (Chen et al., 2019). The bar
851 graph on the right displays the maximal mitotic duration estimated by the fit. Error bars
852 represent 95% confidence intervals of the fitted maximal mitotic duration.
853 **D** Cartoon displays the simplified scheme used to simulate the generation of MCC by the
854 eSAC system.
855 **E** Numerical simulation of the dose-response curves by assuming the assembly of signaling
856 complexes and ultimately the MCC as shown in **D** followed by a model described by He
857 et al (He et al., 2011).

858
859
860

861 **Figure 2**

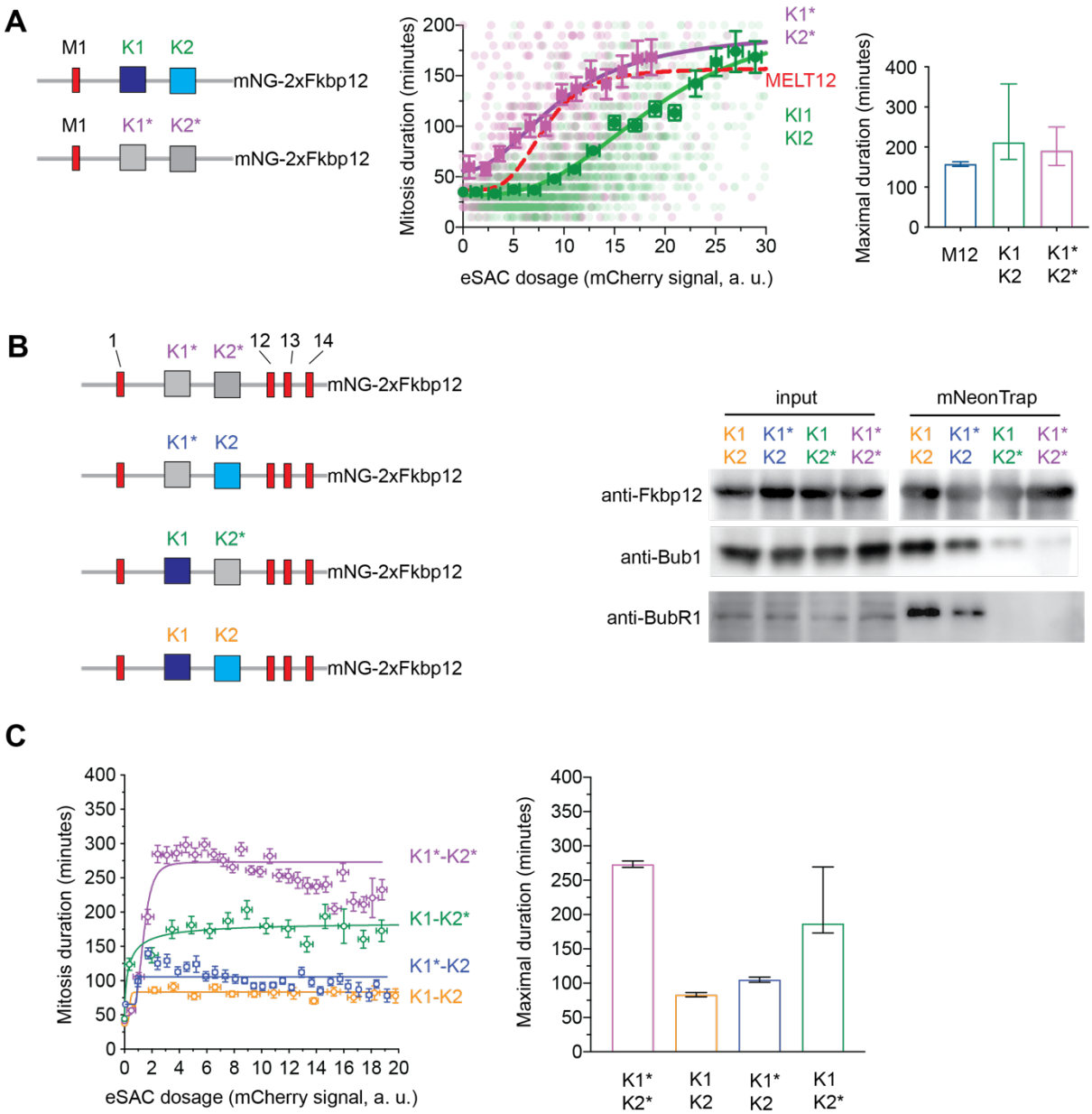

862

863 **Figure 2 Characterization of the binding of the KI motifs in the eSAC phosphodomain with**
864 **Bub1 and BubR1 and its contribution to eSAC signaling.**

865 **A** Left: Schematic of the two phosphodomains used to test whether the KI motifs contribute
866 to MCC assembly mediated by the MELT motif in the eSAC phosphodomain. KI1-KI2
867 indicates phosphodomain with intact KI motifs, KI1*-KI2* indicates phosphodomains
868 wherein the KI motifs are inactivated using suitable point mutations (see Methods for
869 details). The scatter plot in the middle displays the dose-response data for the two
870 phosphodomains (n = 1888 for KI1-KI2 (green) and n = 836 for KI1*-KI2* (magenta) from

871 ≥ 2 experiments; symbol usage follows the scheme established in 1**C**). The bar graph on
872 the right displays the maximal mitotic duration predicted by 4-parameter sigmoidal fits to
873 the binned mean values as in Figure 1C. Vertical lines display 95% confidence intervals
874 on the fit parameter.

875 **B** Left: Schematic of the phosphodomains consisting of 4 MELT motifs and either active or
876 inactive (indicated by *) KI motifs. Right: Immunoprecipitation of the eSAC
877 phosphodomains using mNeonGreen-Trap beads followed by immunoblot analysis to
878 probe for the co-IP of the indicated proteins.

879 **C** Dose-response data for the indicated phosphodomains. Only the mean values of binned
880 data are shown for clarity. Data analysis performed as in 1D (n = 1019, 1024, 666, and
881 3219 from ≥ 2 experiments for KI1-KI2, KI1-KI2*, KI1*-K2, and KI1*-KI2* respectively).
882 The bar graph on the right displays the maximal time in mitosis of the fitted maximal mitotic
883 duration (error bars represent 95% confidence intervals).

884 **Figure 3**

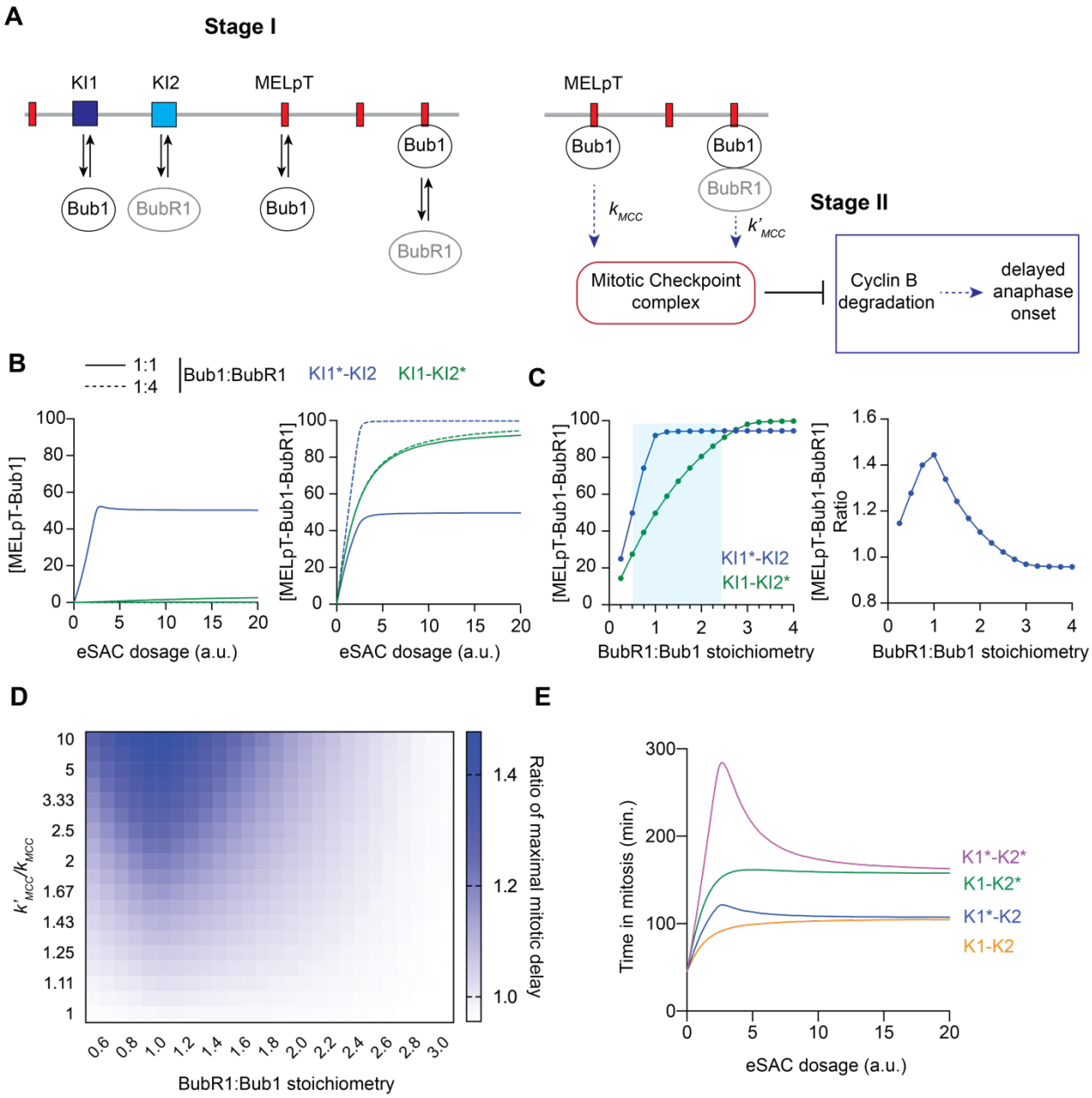

885

886 **Figure 3 Numerical simulation of the dose-response data for the eSAC phosphodomains**
887 **containing KI motifs.**

888 **A** Schematic of the two-stage model used to simulate the dose-response curves.

889 **B** The influence of Bub1-BubR1 stoichiometry and the differential sequestration of Bub1 and
890 BubR1 by the KI motifs on the equilibrium concentrations of the two signaling complexes
891 formed on phosphorylated MELT motifs.

892 **C** Comparison of the equilibrium concentration of the MELpT-Bub1-BubR1 complex
893 assembled by KI1*-KI2 and KI1-KI2* (left) and the ratio (right) of their maximal responses
894 as a function of the Bub1-BubR1 stoichiometry. For the two phosphodomains to generate
895 different responses, the Bub1-BubR1 stoichiometry must be around 1:1 (indicated by the
896 blue shaded area).
897 **D** The ratio of the maximal responses produced by KI1*-KI2 and KI1-KI2* as a function of
898 the Bub1-BubR1 stoichiometry and the ratio of the rates at which the MELpT-Bub1-BubR1
899 and the MELpT-Bub1 signaling complexes produce MCC (i.e., k'_{MCC}/k_{MCC}).
900 **E** Simulation of the dose-response curves for the four phosphodomains using the same set
901 of parameter values.

902

903 **Figure 4**

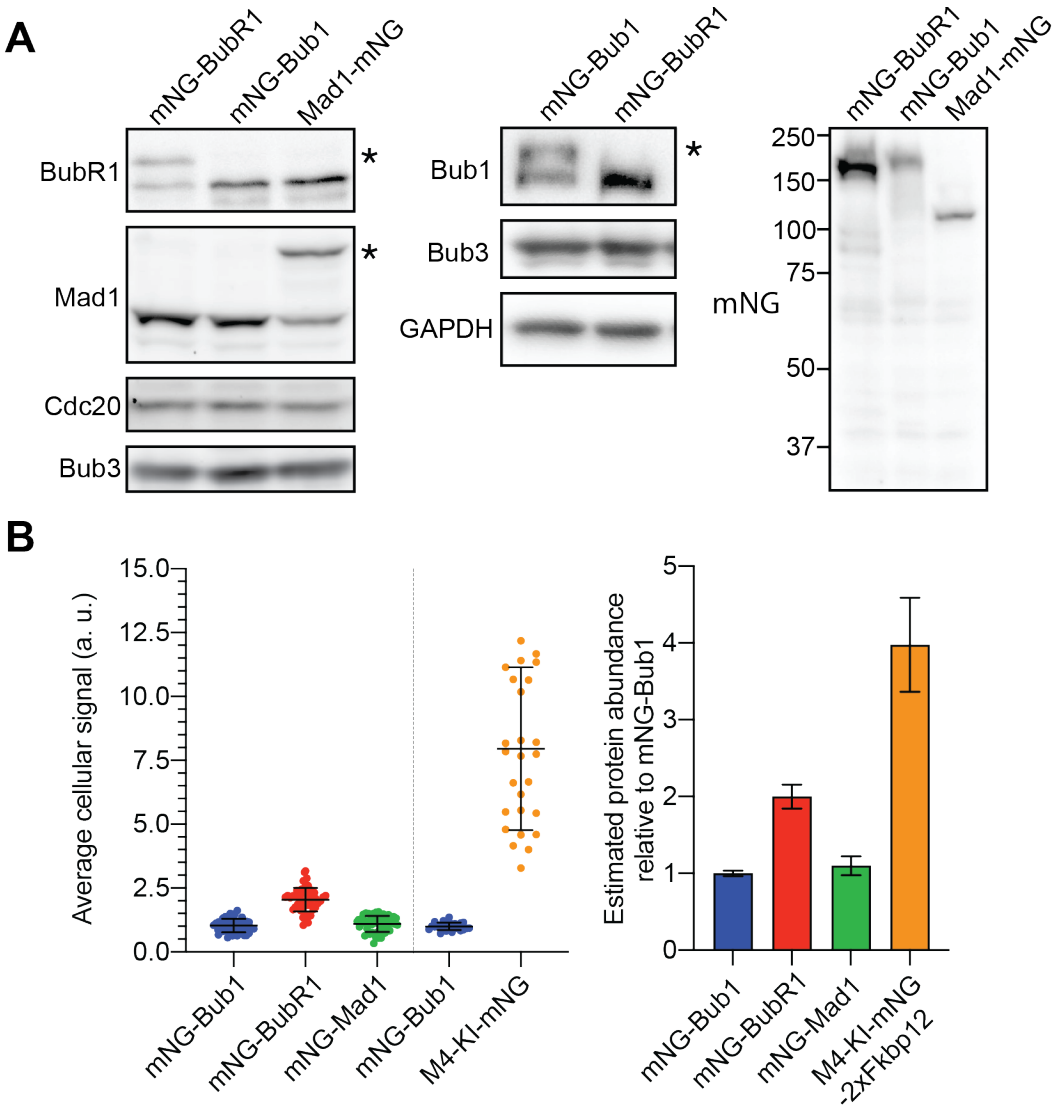

904

905 **Figure 4 Quantification of the relative abundance of a eSAC phosphodomain,**
906 **mNeonGreen-Bub1, mNeonGreen-BubR1, and Mad1-mNeonGreen in genome-edited HeLa**
907 **cell lines.**

908 **A** Immunoblots showing that roughly half of BubR1 and Mad1 (left) and Bub1 (middle)
909 proteins in the three partially genome-edited cell lines is tagged with mNeonGreen
910 (asterisks on the right of each displayed blot mark the mNG fusion protein). Immunoblot
911 on the right shows whole-cell extracts of the three cell lines probed with anti-mNeonGreen
912 antibodies.

913 **B** Average mNG-Bub1, mNG-BubR1, Mad1-mNG, and M4-KI1-KI2-mNG-2xFkbp12 signals
914 from mitotic HeLa cells (left) and estimation of the relative protein abundance, assuming

915 that the total protein abundance is twice as high as the abundance of the mNG-labeled
916 species (mean ± std. dev.).

917

918 **Figure 5**

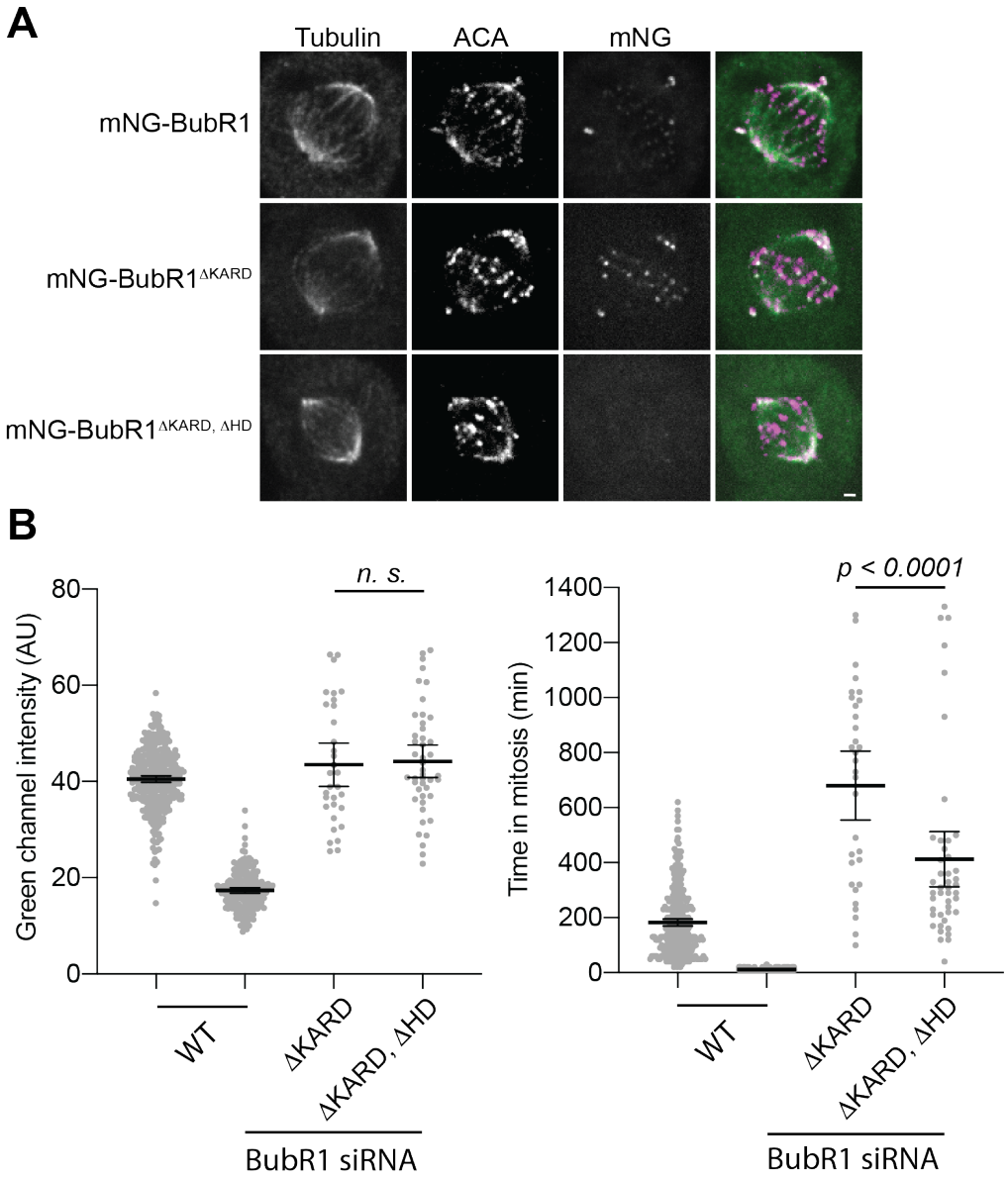

919

920 **Figure 5 Recruitment of BubR1 by Bub1 per se contributes to the activity of the**
921 **kinetochore-based SAC signaling.**

922 **A** Micrographs of representative cells displaying the indicated antigens at the top. The top
923 row displays micrographs of the partially genome-edited cell line expressing mNG-BubR1.
924 The bottom two rows display representative cells after endogenous BubR1 was knocked
925 down and the indicated mutant, mNG-tagged version was ectopically expressed (scale
926 bar ~ 1.22 microns).

927 **B** Scatterplot on the left displays the duration of mitosis of either genome-edited *mNG-*
928 *BUBR1* or cells that ectopically expressed the indicated mutant after treatment with BubR1

929 siRNA in media containing 25 nM nocodazole. Scatterplot on the right displays the
930 average cytosolic mNeonGreen signal from the same cells (mean ± 95% confidence
931 intervals).

932

933 **Supplementary Figure 1**

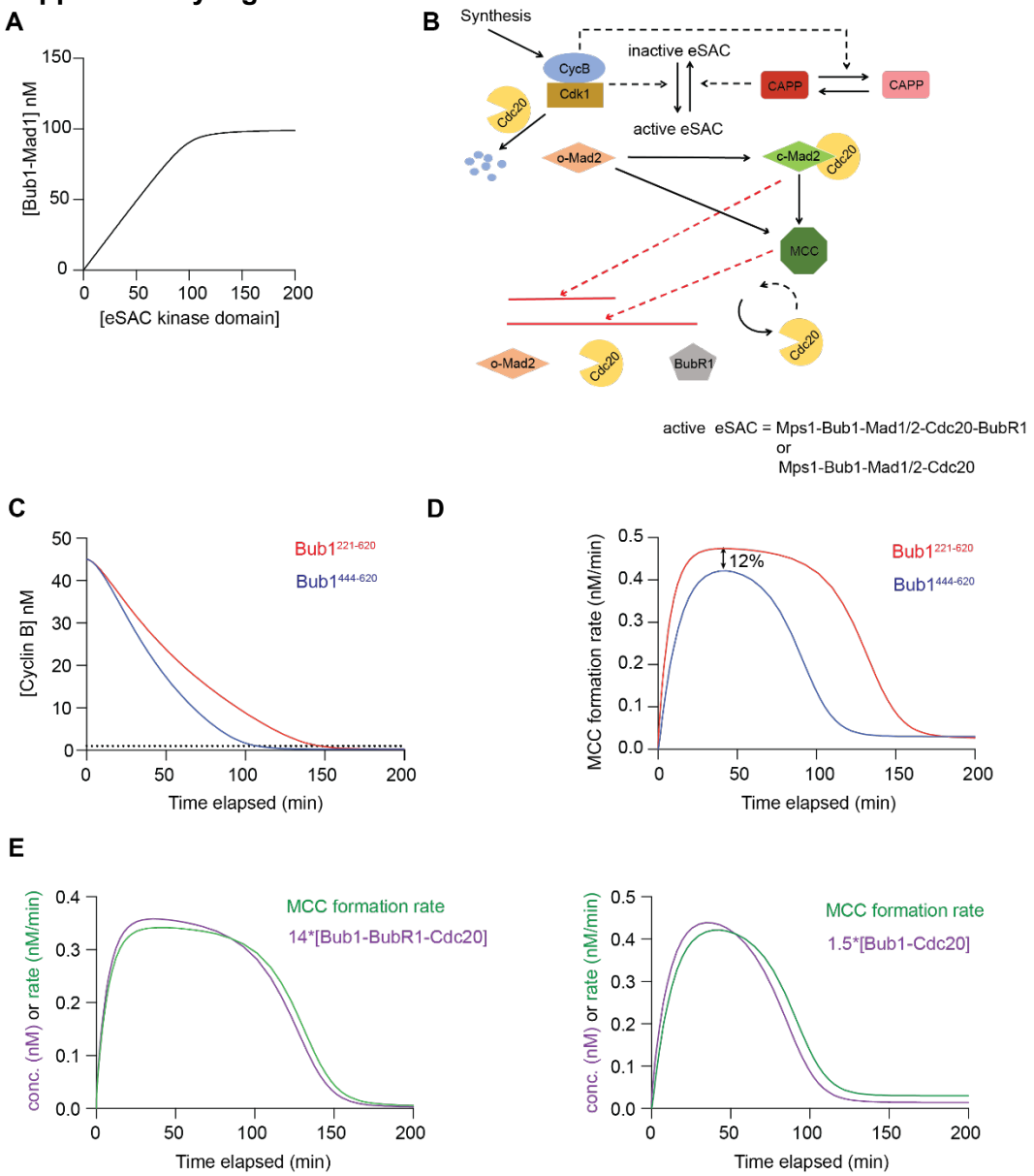

934
935
936 **Figure S1 Simulation of the dose-response curves for the Bub1 eSAC system.**

937 **A** The amount of the eSAC signaling complex (Bub1-Mad1) saturates due to the limited
938 availability of Mad1 (100 nM).

939 **B** Schematic of the model used to simulate the dose-response data for the "full" and
940 "truncated" Bub1 phosphodomain used in the eSAC system.

941 **C** Temporal evolution of Cyclin B concentration for the two eSAC systems.

942 **D** Assessment of MCC formation rates for the full and truncated phosphodomain.

943 **E** Superimposition of the dynamics of the MCC formation rate and the concentration of
944 signaling complexes that produce MCC. Note that the ~ 10-fold difference in the scaling

in the two panels used for displaying with clarity the concentrations of the signaling complex.

948 **Supplementary Figure 2**

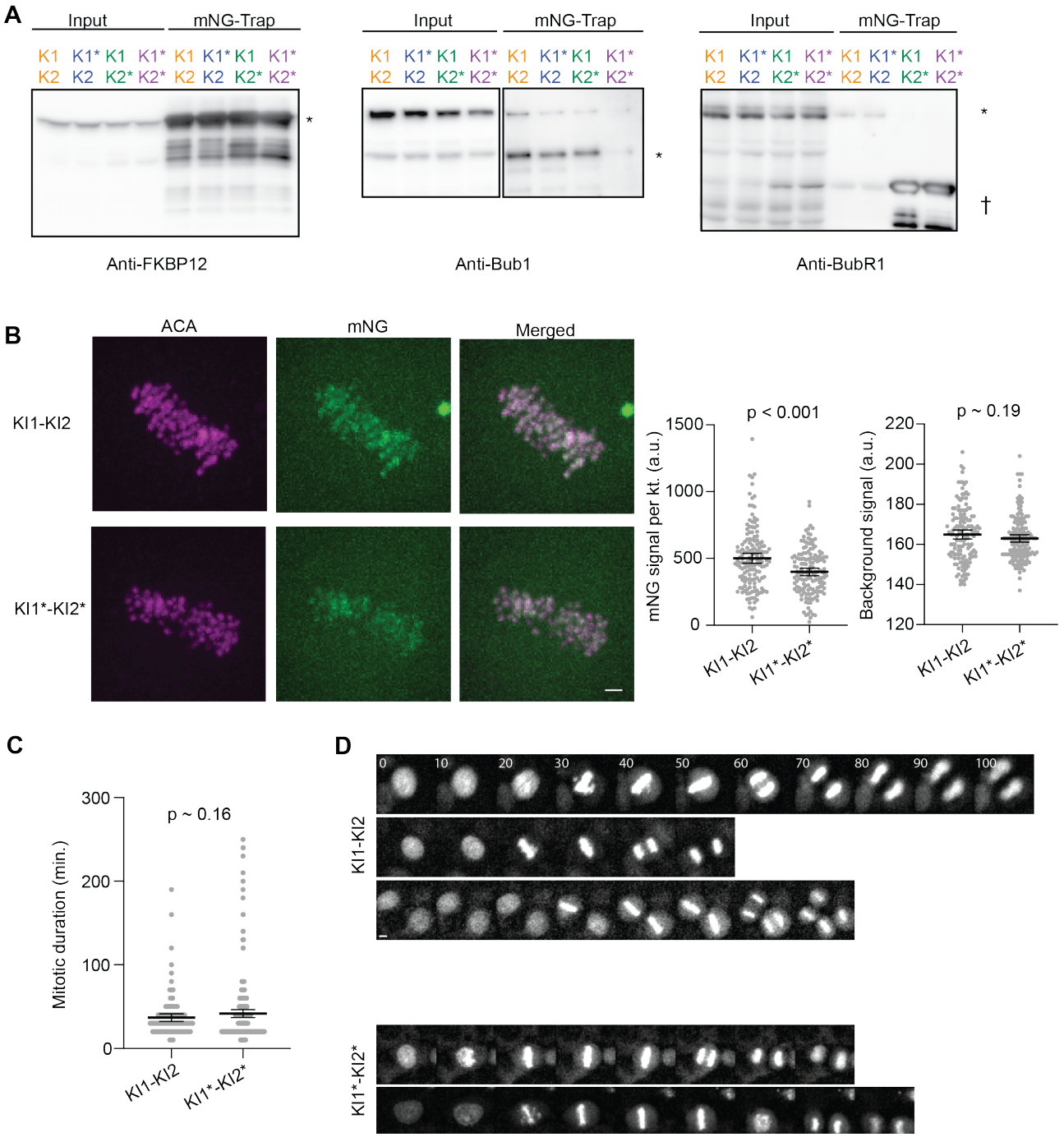

949

950

951

952 **Supplementary Figure 2 Characterization of the interactions of the KI-motif containing**

953 **phosphodomains with Bub1 and BubR1 and their cellular localization**

954 **A** Immunoblots probing for the indicated protein for assessing the co-immunoprecipitation of
955 Bub1 and BubR1 with the indicated eSAC phosphodomain (at the top). The asterisk marks
956 the position of the band corresponding to the full-length protein. The cross marks bands
957 may be degradation products of BubR1.
958 **B** Left: Representative micrographs of metaphase cells displaying the indicated proteins
959 (scale bar ~ 1.1 μm). Right: Quantification of kinetochore-localized mNG signal
960 corresponding to the indicated phosphodomain (n = 149, 147 for KI1-KI2 and KI1*-KI2*
961 respectively). The scatterplot on the right displays the background intensity measured in
962 a 12x12 pixel box concentric with the 6x6 box corresponding to the kinetochore spot. The
963 p-values indicate the results of Welch's t-test. Similar mean values of the background
964 fluorescence, which is indicative of the expression level of the phosphodomain, indicate
965 that the difference in the kinetochore-localized phosphodomain is not due to a difference
966 in the expression level.
967 **C** Duration of mitosis of untreated cells expressing KI1-KI2-mNG-2xFkbp12 or KI1*-KI2*-
968 mNG-2xFkbp12 along with Frb-mCherry-Mps1$^{500-817}$ in the absence of Rapamycin (n =
969 124, 175 from 2 experiments for KI1-KI2 and KI1*-KI2* respectively). The p-value
970 indicates the result of Welch's t-test.
971 **D** Selected montages show mitotic progression of the indicated HeLa cell lines transiently
972 transfected with mNG-H2B expression plasmids. (scale bar ~ 4.87 μm). Numbers at the
973 top left corner indicate the time elapsed in minutes from the first frame.

974

975 **Supplementary Figure 3**
976

A

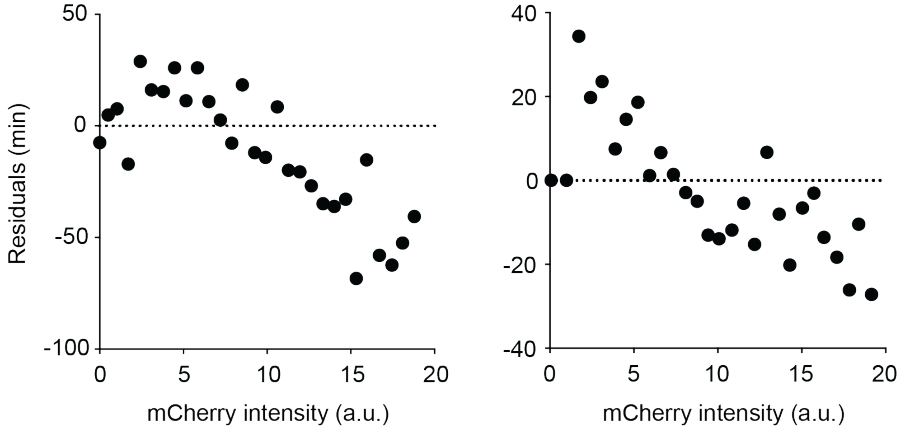

B

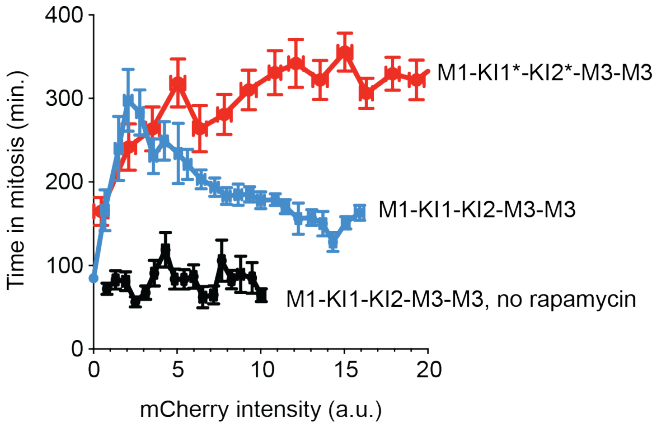

977
978
979 **Figure S3 Non-monotonic nature of the dose-response curves and dose-response data for**
980 **phosphodomains containing the two KI motifs along with seven MELT motifs**

981 **A** Residual plots from a 4-parameter sigmoidal fit to the dose-response data for the KI1*-
982 KI2* (left) and KI1-KI2* (right) phosphodomains.

983 **B** Dose-response data for the indicated phosphodomains. Circles represent average values
984 of binned data (vertical and horizontal lines display standard error on each mean value.
985 n= 498, 1313, and 394 respectively for M1-KI1-KI2-M3-M3, M1-KI1*-KI2*-M3-M3, and M1-
986 KI1-KI2-M3-M3 without Rapamycin respectively pooled from two or more experiments).

987
988
989

990

991 **Supplementary Figure S4**

992

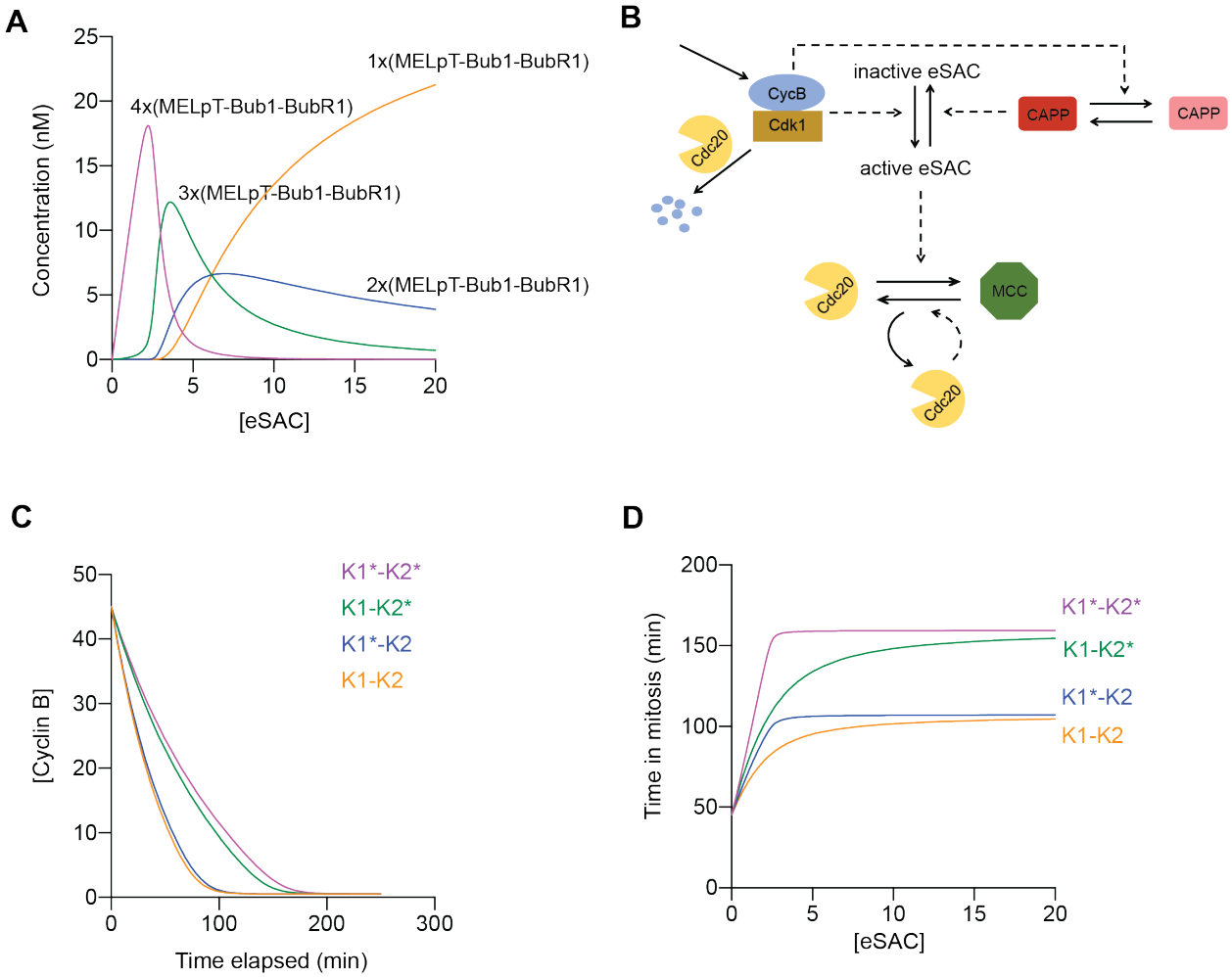

993

994 **Supplementary Figure S4 Simulation of the dose-response data for eSAC systems**
995 **containing the KI motifs and MELT motifs.**

996 **A** Abundance of the indicated eSAC signaling complex (of the form n*(MELpT-Bub1-
997 BubR1)) as a function of the total concentration of the eSAC activator complex. The
998 number n indicates the number of MELT motifs bound to Bub1-BubR1. Also see Table
999 S3.

1000 **B** Schematic of the model used to simulate the dose-response data for eSAC with MELT
1001 and KI motifs.

1002 **C** Temporal evolution of Cyclin B concentration for the MELT and KI motif eSAC system.

1003 **D** Simulation of dose-response curves for the four phosphodomains without synergistic
1004 interactions between the MELT motifs.

1005

1006 **References**

1007 Aravamudhan, P., A.A. Goldfarb, and A.P. Joglekar. 2015. The kinetochore encodes a mechanical
1008 switch to disrupt spindle assembly checkpoint signalling. *Nat Cell Biol*. 17:868-879.
1009 Bolanos-Garcia, V.M., T. Lischetti, D. Matak-Vinkovic, E. Cota, P.J. Simpson, D.Y. Chirgadze, D.R.
1010 Spring, C.V. Robinson, J. Nilsson, and T.L. Blundell. 2011a. Structure of a Blinkin-BUBR1
1011 complex reveals an interaction crucial for kinetochore-mitotic checkpoint regulation via
1012 an unanticipated binding Site. *Structure*. 19:1691-1700.
1013 Bolanos-Garcia, Victor M., T. Lischetti, D. Matak-Vinković, E. Cota, Pete J. Simpson, Dimitri Y.
1014 Chirgadze, David R. Spring, Carol V. Robinson, J. Nilsson, and Tom L. Blundell. 2011b.
1015 Structure of a Blinkin-BUBR1 Complex Reveals an Interaction Crucial for Kinetochore-
1016 Mitotic Checkpoint Regulation via an Unanticipated Binding Site. *Structure*. 19:1691-
1017 1700.
1018 Bouchoux, C., and F. Uhlmann. 2011. A quantitative model for ordered Cdk substrate
1019 dephosphorylation during mitotic exit. *Cell*. 147:803-814.
1020 Chen, C., I.P. Whitney, A. Banerjee, C. Sacristan, P. Sekhri, D.M. Kern, A. Fontan, G. Kops, J.J.
1021 Tyson, I.M. Cheeseman, and A.P. Joglekar. 2019. Ectopic Activation of the Spindle
1022 Assembly Checkpoint Signaling Cascade Reveals Its Biochemical Design. *Curr Biol*. 29:104-
1023 119 e110.
1024 Collin, P., O. Nashchekina, R. Walker, and J. Pines. 2013. The spindle assembly checkpoint works
1025 like a rheostat rather than a toggle switch. *Nat Cell Biol*. 15:1378-1385.
1026 Di Fiore, B., Norman E. Davey, A. Hagting, D. Izawa, J. Mansfeld, Toby J. Gibson, and J. Pines. 2015.
1027 The ABBA Motif Binds APC/C Activators and Is Shared by APC/C Substrates and
1028 Regulators. *Developmental Cell*. 32:358-372.
1029 Dick, A.E., and D.W. Gerlich. 2013. Kinetic framework of spindle assembly checkpoint signalling.
1030 *Nat Cell Biol*. 15:1370-1377.
1031 Elowe, S., S. Hummer, A. Uldschmid, X. Li, and E.A. Nigg. 2007. Tension-sensitive Plk1
1032 phosphorylation on BubR1 regulates the stability of kinetochore microtubule
1033 interactions. *Genes Dev*. 21:2205-2219.
1034 Espert, A., P. Uluocak, R.N. Bastos, D. Mangat, P. Graab, and U. Gruneberg. 2014. PP2A-B56
1035 opposes Mps1 phosphorylation of Knl1 and thereby promotes spindle assembly
1036 checkpoint silencing. *J Cell Biol*. 206:833-842.
1037 Faesen, A.C., M. Thanasoula, S. Maffini, C. Breit, F. Muller, S. van Gerwen, T. Bange, and A.
1038 Musacchio. 2017. Basis of catalytic assembly of the mitotic checkpoint complex. *Nature*.
1039 Foley, E.A., M. Maldonado, and T.M. Kapoor. 2011. Formation of stable attachments between
1040 kinetochores and microtubules depends on the B56-PP2A phosphatase. *Nat Cell Biol*.
1041 13:1265-1271.
1042 Hayward, D., J. Bancroft, D. Mangat, T. Alfonso-Perez, S. Dugdale, J. McCarthy, F.A. Barr, and U.
1043 Gruneberg. 2019. Checkpoint signaling and error correction require regulation of the
1044 MPS1 T-loop by PP2A-B56. *J Cell Biol*. 218:3188-3199.
1045 He, E., O. Kapuy, R.A. Oliveira, F. Uhlmann, J.J. Tyson, and B. Novák. 2011. System-level feedbacks
1046 make the anaphase switch irreversible. *Proceedings of the National Academy of Sciences*.
1047 Ji, Z., H. Gao, L. Jia, B. Li, and H. Yu. 2017. A sequential multi-target Mps1 phosphorylation cascade
1048 promotes spindle checkpoint signaling. *Elife*. 6.

1049 Jia, L., B. Li, and H. Yu. 2016. The Bub1-Plk1 kinase complex promotes spindle checkpoint
1050 signalling through Cdc20 phosphorylation. *Nat Commun*. 7:10818.
1051 Kern, D.M., T. Kim, M. Rigney, N. Hattersley, A. Desai, and I.M. Cheeseman. 2015. The outer
1052 kinetochore protein KNL-1 contains a defined oligomerization domain in nematodes. *Mol*
1053 *Biol Cell*. 26:229-237.
1054 Khandelia, P., K. Yap, and E.V. Makeyev. 2011. Streamlined platform for short hairpin RNA
1055 interference and transgenesis in cultured mammalian cells. *Proc Natl Acad Sci USA*.
1056 108:12799-12804.
1057 Kiyomitsu, T., H. Murakami, and M. Yanagida. 2011. Protein interaction domain mapping of
1058 human kinetochore protein Blinkin reveals a consensus motif for binding of spindle
1059 assembly checkpoint proteins Bub1 and BubR1. *Mol Cell Biol*. 31:998-1011.
1060 Krenn, V., K. Overlack, I. Primorac, S. van Gerwen, and A. Musacchio. 2014. KI motifs of human
1061 Knl1 enhance assembly of comprehensive spindle checkpoint complexes around MELT
1062 repeats. *Curr Biol*. 24:29-39.
1063 Krenn, V., A. Wehenkel, X. Li, S. Santaguida, and A. Musacchio. 2012. Structural analysis reveals
1064 features of the spindle checkpoint kinase Bub1-kinetochore subunit Knl1 interaction. *J*
1065 *Cell Biol*. 196:451-467.
1066 Kruse, T., G. Zhang, M.S. Larsen, T. Lischetti, W. Streicher, T. Kragh Nielsen, S.P. Bjorn, and J.
1067 Nilsson. 2013. Direct binding between BubR1 and B56-PP2A phosphatase complexes
1068 regulate mitotic progression. *J Cell Sci*. 126:1086-1092.
1069 Lara-Gonzalez, P., T. Kim, K. Oegema, K. Corbett, and A. Desai. 2021a. A tripartite mechanism
1070 catalyzes Mad2-Cdc20 assembly at unattached kinetochores. *Science*. 371:64-67.
1071 Lara-Gonzalez, P., J. Pines, and A. Desai. 2021b. Spindle assembly checkpoint activation and
1072 silencing at kinetochores. *Semin. Cell Dev. Biol.* 117:86-98.
1073 Leontiou, I., N. London, K.M. May, Y. Ma, L. Grzesiak, B. Medina-Pritchard, P. Amin, A.A.
1074 Jeyaprakash, S. Biggins, and K.G. Hardwick. 2019. The Bub1-TPR Domain Interacts Directly
1075 with Mad3 to Generate Robust Spindle Checkpoint Arrest. *Curr Biol*. 29:2407-2414 e2407.
1076 Musacchio, A. 2015. The Molecular Biology of Spindle Assembly Checkpoint Signaling Dynamics.
1077 *Curr Biol*. 25:R1002-1018.
1078 Nijenhuis, W., G. Vallardi, A. Teixeira, G.J. Kops, and A.T. Saurin. 2014. Negative feedback at
1079 kinetochores underlies a responsive spindle checkpoint signal. *Nat Cell Biol*. 16:1257-
1080 1264.
1081 Overlack, K., T. Bange, F. Weissmann, A.C. Faesen, S. Maffini, I. Primorac, F. Muller, J.M. Peters,
1082 and A. Musacchio. 2017. BubR1 Promotes Bub3-Dependent APC/C Inhibition during
1083 Spindle Assembly Checkpoint Signaling. *Curr Biol*. 27:2915-2927 e2917.
1084 Overlack, K., I. Primorac, M. Vleugel, V. Krenn, S. Maffini, I. Hoffmann, G.J. Kops, and A.
1085 Musacchio. 2015. A molecular basis for the differential roles of Bub1 and BubR1 in the
1086 spindle assembly checkpoint. *Elife*. 4:e05269.
1087 Piano, V., A. Alex, P. Stege, S. Maffini, G.A. Stoppiello, P.J. Huis In 't Veld, I.R. Vetter, and A.
1088 Musacchio. 2021. CDC20 assists its catalytic incorporation in the mitotic checkpoint
1089 complex. *Science*. 371:67-71.
1090 Primorac, I., J.R. Weir, E. Chiroli, F. Gross, I. Hoffmann, S. van Gerwen, A. Ciliberto, and A.
1091 Musacchio. 2013. Bub3 reads phosphorylated MELT repeats to promote spindle assembly
1092 checkpoint signaling. *Elife*. 2:e01030.

1093 Qian, J., M.A. Garcia-Gimeno, M. Beullens, M.G. Manzione, G. Van der Hoeven, J.C. Igual, M.
1094 Heredia, P. Sanz, L. Gelens, and M. Bollen. 2017. An Attachment-Independent Biochemical
1095 Timer of the Spindle Assembly Checkpoint. *Mol Cell*. 68:715-730 e715.
1096 Roy, B., S.J.Y. Han, A.N. Fontan, S. Jema, and A.P. Joglekar. 2022. Aurora B phosphorylates Bub1
1097 to promote spindle assembly checkpoint signaling. *Curr Biol*. 32:237-247 e236.
1098 Roy, B., S.J.Y. Han, A.N. Fontan, and A.P. Joglekar. 2020. The copy-number and varied strength of
1099 MELT motifs in Spc105 balance the strength and responsiveness of the Spindle Assembly
1100 Checkpoint. *Elife*. 9.
1101 Saurin, A.T., M.S. van der Waal, R.H. Medema, S.M. Lens, and G.J. Kops. 2011. Aurora B
1102 potentiates Mps1 activation to ensure rapid checkpoint establishment at the onset of
1103 mitosis. *Nat Commun*. 2:316.
1104 Suijkerbuijk, S.J., M. Vleugel, A. Teixeira, and G.J. Kops. 2012. Integration of kinase and
1105 phosphatase activities by BUBR1 ensures formation of stable kinetochore-microtubule
1106 attachments. *Dev Cell*. 23:745-755.
1107 Sullivan, M., T. Higuchi, V.L. Katis, and F. Uhlmann. 2004. Cdc14 phosphatase induces rDNA
1108 condensation and resolves cohesin-independent cohesion during budding yeast
1109 anaphase. *Cell*. 117:471-482.
1110 Taylor, S.S., E. Ha, and F. McKeon. 1998. The human homologue of Bub3 is required for
1111 kinetochore localization of Bub1 and a Mad3/Bub1-related protein kinase. *J Cell Biol*.
1112 142:1-11.
1113 Taylor, S.S., D. Hussein, Y. Wang, S. Elderkin, and C.J. Morrow. 2001. Kinetochore localisation and
1114 phosphorylation of the mitotic checkpoint components Bub1 and BubR1 are differentially
1115 regulated by spindle events in human cells. *J Cell Sci*. 114:4385-4395.
1116 Tromer, E., D. Bade, B. Snel, and G.J. Kops. 2016. Phylogenomics-guided discovery of a novel
1117 conserved cassette of short linear motifs in BubR1 essential for the spindle checkpoint.
1118 *Open Biol*. 6.
1119 Vleugel, M., M. Omerzu, V. Groenewold, M.A. Hadders, S.M. Lens, and G.J. Kops. 2015. Sequential
1120 multisite phospho-regulation of KNL1-BUB3 interfaces at mitotic kinetochores. *Mol Cell*.
1121 57:824-835.
1122 Vleugel, M., E. Tromer, M. Omerzu, V. Groenewold, W. Nijenhuis, B. Snel, and G.J. Kops. 2013.
1123 Arrayed BUB recruitment modules in the kinetochore scaffold KNL1 promote accurate
1124 chromosome segregation. *J Cell Biol*. 203:943-955.
1125 von Schubert, C., F. Cubizolles, Jasmine M. Bracher, T. Sliedrecht, Geert J.P.L. Kops, and Erich A.
1126 Nigg. 2015. Plk1 and Mps1 Cooperatively Regulate the Spindle Assembly Checkpoint in
1127 Human Cells. *Cell Reports*. 12:66-78.
1128 Wang, J., Z. Wang, T. Yu, H. Yang, D.M. Virshup, G.J.P.L. Kops, S.H. Lee, W. Zhou, X. Li, W. Xu, and
1129 Z. Rao. 2016a. Crystal structure of a PP2A B56-BubR1 complex and its implications for
1130 PP2A substrate recruitment and localization. *Protein & Cell*. 7:516-526.
1131 Wang, X., R. Bajaj, M. Bollen, W. Peti, and R. Page. 2016b. Expanding the PP2A Interactome by
1132 Defining a B56-Specific SLiM. *Structure*. 24:2174-2181.
1133 Yuan, I., I. Leontiou, P. Amin, K.M. May, S. Soper Ni Chafraidh, E. Zlamalova, and K.G. Hardwick.
1134 2017. Generation of a Spindle Checkpoint Arrest from Synthetic Signaling Assemblies.
1135 *Curr Biol*. 27:137-143.

1136 Zhang, G., T. Lischetti, D.G. Hayward, and J. Nilsson. 2015. Distinct domains in Bub1 localize RZZ
1137 and BubR1 to kinetochores to regulate the checkpoint. *Nat Commun*. 6:7162.
1138 Zhang, G., T. Lischetti, and J. Nilsson. 2014. A minimal number of MELT repeats supports all the
1139 functions of KNL1 in chromosome segregation. *J Cell Sci*. 127:871-884.
1140 Zhang, G., B.L. Mendez, G.G. Sedgwick, and J. Nilsson. 2016. Two functionally distinct kinetochore
1141 pools of BubR1 ensure accurate chromosome segregation. *Nat Commun*. 7:12256.
1142